Intramolecular self-organised structures in amphiphilic (co)polymers

Peter Košovan

Intramolecular self-organised structures in amphiphilic (co)polymers

Peter Košovan

Dissertation

Supervisor: Karel Procházka

Co-supervisor: Zuzana Limpouchová

October 2009

Department of Physical and Macromolecular Chemistry

Faculty of Science, Charles University in Prague

Czech Republic

Lorem ipsum dolor sit amet, consectetur adipisicing elit, sed do eiusmod tempor incididunt ut labore et dolore magna aliqua. Ut enim ad minim veniam, quis nostrud exercitation ullamco laboris nisi ut aliquip ex ea commodo consequat. Duis aute irure dolor in reprehenderit in voluptate velit esse cillum dolore eu fugiat nulla pariatur. Excepteur sint occaecat cupidatat non proident, sunt in culpa qui officia deserunt mollit anim id est laborum.

Lorem Ipsum je demonstrativní výplňový text používaný v tiskařském a knihařském průmyslu. Lorem Ipsum je považováno za standard v této oblasti už od začátku 16. století, kdy dnes neznámý tiskař vzal kusy textu a na jejich základě vytvořil speciální vzorovou knihu. Jeho odkaz nevydržel pouze pět století, on přežil i nástup elektronické sazby v podstatě beze změny. Nejvíce popularizováno bylo Lorem Ipsum v šedesátých letech 20. století, kdy byly vydávány speciální vzorníky s jeho pasážemi a později pak díky počítačovým DTP programům jako Aldus PageMaker.

`http://cs.lipsum.com`

Contents

Abstract

This dissertation presents an overview of our computer simulation studies of the conformational behaviour of amphiphilic polymers. In the studies we showed that the polymers form a variety of self-organised structures at a single molecule level. These include the pearl-necklace structure, spherical and cylindrical intramolecular micelles and bundles. From the simulations we were able to obtain a deeper insight into the behaviour of amphiphilic polymers. Some of the results were compared to experimental or theoretical studies of similar polymers. In some cases the simulations confirmed earlier interpretations which were based on analogy or intuition. In other cases they revealed new phenomena which had not been considered before.

Abbreviations and symbols used in the text

A	pre-exponential factor
α	degree of dissociation / degree of charging
CG	coarse-graining
DP	Degree of polymerisation
e	elementary charge
ϵ_{LJ}	solvent quality / hydrophobicity / depth of the Lennard-Jones potential
ε_0	permittivity of free space
ε_{r}	relative permittivity
$\mathbf{F}$	force
FENE	Finite-extension nonlinear elastic potential
I	fluorescence intensity
k_{B}	Boltzmann constant
K_{FENE}	stiffness constant of the FENE potential
λ_{B}	Bjerrum length
LJ	Lennard-Jones potential
m	mass of a particle
m	side-chain length of a comb-like copolymer
MC	Monte Carlo simulation method
MD	Molecular Dynamics simulation method
$\vec{\mu}_{\mathrm{A}}$	absorption dipole moment
$\vec{\mu}_{\mathrm{E}}$	emission dipole moment
n	spacing between the side-chains of a comb-like copolymer
N	chain length (number of segments)
ν	scaling exponent
N_{B}	backbone length of a comb-like polymer
PE	polyelectrolyte
PMA	poly(methacrylic acid)
r	distance
$r(t)$	time-resolved fluorescence anisotropy
$\vec{r}_i$	bond vector of the bond between particle i and $i+1$
$\mathbf{r}$	position vector
R_{c}	cutoff radius of the LJ potential
R_{FENE}	cutoff radius of the FENE potential
R_{g}	radius of gyration
R_{HC}	hard-core radius
t	time
T	temperature
$U(r)$	pair potential
v	excluded volume of the monomer unit in good solvent

Introduction

In this work we present an overview of our simulation works concerning the formation of self-organised structures in amphiphilic macromolecules.

This thesis presents an overview of simulation works published by the author of the thesis which concern the formation of self-organised structures in amphiphilic macromolecules. Some other simulation studies to which the author has contributed have not been included here because they do not fit into this framework. Most of the presented simulations deal in one way or another with the formation of pearl-necklace structures. The understanding of the matter has gradually developed over the years and has become much deeper especially after our cooperation with the theoreticians has become more intensive.

The large family of amphiphilic copolymers comprises a variety of otherwise rather loosely related compounds. The word amphiphilic comes from Greek and literally means "loving both". In connection with polymers it refers to macromolecules which contain some parts which have high affinity for the solvent (solvophilic) and others which have low affinity for the solvent (solvophobic). Since in many cases the solvent of interest is water, in this thesis often the terms hydrophilic and hydrophobic will be used for the former and the latter, respectively. Even though it is not strictly correct, at least on the semi-quantitative level the nature of the interaction is the same whether the solvent is water or not. More importantly, it facilitates the connection with biological sciences in which the term *hydrophobic interactions* is used to describe the solvophobic interactions in aqueous environment. All results presented in this thesis have been obtained for generic models of synthetic polymers. Nevertheless, a significant portion of them can be used to explain analogous effects in biopolymers. Behaviour of a complex system, such as an amphiphilic polymer, is determined by a number of mutually interdependent factors. In such system it may be very difficult to identify which of the factors (if any) are the most important and what are the relations between them and the resulting behaviour. Studying a generic model system which possesses key features of the original system may help to solve the problem. Generic models usually contain relatively low number of parameters and it is much easier to identify the influence of each of them. Conclusions obtained for the generic models can then be with some care extrapolated to explain the behaviour of the original complex system. From the investigation of the generic model it may also be possible to identify which features of the behaviour are universal and which stem from some specific interactions. In this way we have implicitly defined what we mean by a specific interaction: any effect which cannot be observed in a generic qualitative model. Therefore, depending on the model we refer to, the term specific interaction may mean slightly different things.

Since the early years of macromolecular science the ideal chain model has been one of the few models for which analytical solutions have been found [1]. The success of this model was due to a fortuitous cancellation of errors coming from different approximations. If the solvophobic attraction among the monomer units is exactly cancelled by the steric repulsion, the polymer follows the statistics of the ideal chain. The state of such polymer is called the theta state and serves as the standard state in polymer science. The solvophobic interaction is temperature-dependent and hence for a particular polymer-solvent combination, the theta state can be realised at a certain temperature (theta temperature, theta solvent). However, for many polymer-solvent combinations the theta state cannot be realised at all because some chemical processes prevent it. If the temperature is higher than the theta temperature, the excluded volume interaction prevails and consequently the size of the polymer coil is larger than that of the theta polymer. In such case the polymer is well soluble in the solvent and hence it is referred to as good solvent conditions. On the other hand, if the solvophobic attraction prevails, the polymer collapses into a compact globule which on a macroscopic scale results in precipitation. Such conditions are called poor solvent conditions. The spatial arrangement of polymer chain is called conformation and the good and poor solvent conditions are examples of how the conformation on the molecular scale is linked to the macroscopic properties of solution. Another example of macroscopic changes caused by the conformational changes of individual macromolecules is the denaturation of proteins. The behaviour of neutral homopolymers in dilute solution is nowadays well understood, has been confirmed by a number of experimental and simulation studies and has become an essential part of polymer sciences textbooks [1–4].

In many cases analytical expressions have not been obtained. However, it has been possible to express many important results in the form of a power law, such as that for the radius of gyration,

$$R_{\mathrm{g}} = AN^{\nu} \sim N^{\nu}\,, \tag{1}$$

where R_{g} is the radius of gyration of the polymer, A is the constant pre-factor, N is the number of segments and ν is the scaling exponent. The approaches which predict the power laws and the scaling exponents are known as scaling approaches and over the years they have become a part of the standard toolbox of polymer theory [5].

Specific interactions related to the detailed chemical structure of a given polymer are reflected in the constant pre-factor while the scaling exponent is universal for many polymers which fulfil assumptions of the model. The scaling regime is attained for sufficiently long polymers. However, sufficiently long can mean very different things depending on the topology of the polymer and for finite polymers

deviations from the power law occur. For example, close to theta solvent the power law behaviour is well obeyed for chain length $N \approx 10$ while for star polymers $N \approx 1000$ is necessary [5]. In one of our publications we have shown that for comb-like polymers, it may as well be $N \approx 10^4$ or even more [6]. In such case the scaling behaviour is eventually attained beyond the synthetic limit for the chain length. Hence, for more complicated topologies, the power of the scaling predictions is limited as they only apply to very large systems. In such a case it is desirable to provide also the predictions for finite-size polymers. Usually such predictions cannot be obtained using analytical expressions but still numerical methods can provide the desired data.

It is even more complicated to make theoretical predictions for amphiphilic polymers than in the homopolymer case. Therefore, while the conformational behaviour of linear homopolymers is well understood, this is not the case of amphiphilic polymers. In amphiphilic polymers the solvophobic monomer units tend to stick together and form clusters which is the driving force for aggregation. It is opposed by the repulsion among the solvophilic parts of the amphiphilic polymer which provides the stopping mechanism for the aggregation. The repulsion may be of various origins as will be discussed a few lines further. Equilibrium is attained when the attraction and the repulsion are exactly balanced. When the force which is responsible for the attractive interaction operates on a shorter range than the repulsive one, aggregates of defined size can be formed in equilibrium. Such system then becomes self-organised and has considerably lower entropy than a disorganised system such as the ideal chain. The morphology and size of the aggregates which are formed is determined by the relative strengths of the two counteracting forces which in turn are determined by the interaction with the surrounding environment. The strength of the interactions and hence the behaviour of the polymer can be tuned by external conditions.

In this work we present studies of several types of amphiphilic polymers which exhibit the self-organising behaviour. All our systems are simulated in the dilute solution limit and the self-organised structures are formed on the intramolecular level. The driving force for the formation of aggregates in all our systems consists in the solvophobic attraction among some of the monomer units. The stopping mechanism is provided either by the steric repulsion among the solvophilic parts or by the electrostatic repulsion among the charged groups contained in the polymer or by the combination of both. Such systems may be very difficult to treat using analytical models or scaling approaches. For some of them it has been attempted with various degrees of success, on others it is just a work in progress.

One system for which theoretical models have successfully and correctly predicted the formation of self-organised structures are polyelectrolytes in poor sol-

vents. Polyelectrolytes are polymers containing groups which can be charged under certain conditions. It has been shown by Khokhlov in 1980 [7] that the spherical shape of such polymer globule is unstable and it deforms to a cigar-like shape. Later on, Dobrynin, Rubinstein and Obukhov [8] have shown that at certain conditions also the cigar shape is unstable and it splits into several smaller spherical globules (pearls) connected by strongly stretched parts of the chain (strings), forming the so-called pearl-necklace conformation. Their predictions have been confirmed by a number of simulation studies, e. g. [9, 10].

In 2005 a similar behaviour has been predicted by Borisov and Zhulina for comb-like copolymers in selective solvents [11] which has been augmented and supported by simulation results in our recent paper [12]. Similar predictions for yet another type of polymer – comb-like polyelectrolytes in selective solvents – have been made by ourselves [13] on the basis of computer simulations. The formation of pearl-necklace structures in PE stars in poor solvents has been anticipated by Sandberg et al. but their scaling analysis as well as simulations have shown that bundles of chains rather than pearl-necklaces are formed [14]. Our results which are being prepared for publication have shown that the pearl-necklaces in the stars with low number of arms while at higher number of arms, bundling is preferred [15]. Polymorphism of the intra-molecular structures, including pearl-necklaces has been also observed in recent Monte Carlo simulations of amphiphilic multiblock copolymers in dilute solutions [16].

As can be seen from previous lines, similar type of self-organising behaviour can be observed in various amphiphilic copolymers. We have been studying many of them by computer simulations. In this thesis we present an overview of the results and attempt to draw the reader's attention to common features in different systems which can be considered as universal, at least to a certain extent.

Simulation methods and interaction potentials

Molecular dynamics

Most simulations presented in this thesis were performed using the method of Molecular Dynamics (MD). Currently it is one of the standard simulation methods and has been described in detail in a number of textbooks [17–20]. Here we only make a brief overview of the method and point out some specific topics which are important for further discussion. For more details on the employed simulation techniques we refer the reader to one of the above-mentioned textbooks.

The ultimate goal of a molecular simulation is to compute ensemble averages of certain observables. One of the ways the averages can be obtained is to observe how the system evolves in time. The ensemble averages can then be computed using the ergodic theorem. It assumes that for an observable X its ensemble average is equal to its time-average when the time interval is long enough

$$\langle X \rangle = \lim_{t \to \infty} \frac{1}{t} \int_0^t X(t)\, \mathrm{d}t\,. \tag{2}$$

In other words, in the limit of infinite time interval, the system samples all parts of the phase space with the proper probabilities. For a finite time interval of a real simulation, equality in equation (2) becomes only approximate. Yet if the system is not entrapped in a metastable state, it can sample a representative part of the phase space and hence such simulation can be used to compute the ensemble average of the observable.

In the MD simulation method, a system is defined by a set of particles and interaction potentials between them. For such a system, we compute its evolution in time by numerically solving the classical Newtonian equations of motion

$$m \frac{\mathrm{d}^2 \mathbf{r}_i}{\mathrm{d}t^2} = -\nabla \sum_{j \neq i}^{N} U(r_{ij}) \qquad i = (1, 2, \ldots, N)\,. \tag{3}$$

The above equation represents a set of N parallel differential equations for N interacting particles where $U(r_{ij})$ is the interaction potential between the particles i and j. The whole simulation is usually performed in a simulation box with periodic boundary conditions which helps to overcome the problem of simulating a relatively small system.

An MD simulation can start from an arbitrary initial configuration. The initial configuration may be far from equilibrium and therefore prior to the productive period of the simulation, an equilibration is performed, during which the system approaches equilibrium. This is manifested by a significant time-drift of certain (not necessarily all) observables. At the end of the equilibration period, no time-drift in any of the observables should be observed, i. e. and all observables should fluctuate around their equilibrium values.

Technically, the time average is computed so that after the equilibration has been accomplished, configurations are stored at regular intervals and the ensemble average is computed as a simple average over all stored configurations. When computing averages of the stored data, it has to be born in mind that the MD method yields correlated data and the correlation has to be taken into account, e. g. using one of the methods described in the book of Frenkel and Smit [18].

It should be noted, however, that if a system ends up in a metastable state, it is also manifested by fluctuations of all observables around a constant value. In the limit of infinite time, the system eventually leaves the metastable state and samples the rest of the phase space. Yet the time the simulated system needs to leave the metastable state depends on its dynamical properties and specifically in polymer systems this may be anything ranging from picoseconds to years. Since a typical simulation represents up to a few microseconds of real time, in some systems it may happen that within the time interval of the simulation only the metastable state is simulated. Unfortunately, it is not possible to prove that a simulation has sampled a sufficient portion of the phase space. However, it can be proved using some physical arguments that a particular system is in an arrested state. If such a situation is suspected for a particular system, it has to be thoroughly examined and if the suspicion is confirmed, the simulation results have to be discarded.

MD in implicit solvent, Langevin thermostat

One way of performing simulations of molecules using the MD method is to define chemical bonds and non-bonding interactions among all pairs of atoms. Such models are widely used e. g. in simulations of proteins where the detailed chemical structure is very important. On the other hand, when the system of interest is a synthetic polymer, the situation can be simplified and an effective interaction can be assigned to a larger group of atoms such as one or several monomer units. Most theoretical models of polymers proceed in the same way. Such procedure is referred to as coarse-graining (CG) and its principles are described in more detail e. g. in the book of Binder [21] or review by Praprotnik et al. [22]. The main advantage of the coarse-graining is significant reduction in the number of degrees of freedom and consequently reduction of the computational complexity

of the problem. The disadvantage is the loss of detail. Usually, a generic CG model yields only qualitative or semi-quantitative information which, nevertheless, may be valuable for understanding the underlying mechanisms of some processes and/or development of theoretical models. In recent years, a lot of effort has been devoted to developing systematic CG procedures which would also account for specific interactions, especially in the groups of Kurt Kremer and Florian Müller-Plathe. However, the success of the systematic CG has been so far limited to a few well-behaving systems. For a more detailed discussion of this topic, we refer the reader to a recent review [22].

If the a polymer in dilute solution is studied, most of the system comprises solvent molecules while the actual molecule of interest is only a minor component. Therefore a further step in coarse-graining dilute solution polymer systems is removing solvent molecules. The approach employed in all simulations presented in this thesis is coupling the system to the Langevin thermostat where the solvent molecules are not simulated explicitly but their presence is emulated by two forces which are added to the classical Newtonian equations of motion. The modified equations then read

$$m_i \frac{d^2\mathbf{r}_i}{dt^2} = -\nabla \sum_{j\neq i} U(r_{ij}) + \mathbf{F}_i^D + \mathbf{F}_i^R \,, \tag{4}$$

where $\mathbf{F}_i^D$ and $\mathbf{F}_i^R$ are the dissipative and the random force respectively. The two additional forces are coupled by the following relations:

$$\mathbf{F}_i^D = -m_i \Gamma \frac{d\mathbf{r}_i}{dt} \,, \tag{5}$$

$$\langle \mathbf{F}_i^R(t) \cdot \mathbf{F}_j^R(t') \rangle = 6\Gamma k_B T m_i \delta_{ij} \delta(t-t'); \qquad \langle \mathbf{F}_i^R(t) \rangle = 0 \,. \tag{6}$$

Besides the fact that the two additional forces emulate the collisions with solvent molecules, they also work as a thermostat, i. e. they keep the system at constant temperature T. Because the coupling equations do not provide an exact definition of the random force, certain level of arbitrariness is left in its choice. A common but not a unique choice is to take $\mathbf{F}^R$ from Gaussian distribution. It can be shown that the system which follows the above-mentioned set of equations samples the canonical ensemble [17, 19].

Although the Langevin thermostat, and implicit solvent methods in general, are very useful simulation tools, there are several problems related to their use.

For example, the random force acts on all particles while in reality collisions with solvent molecules are not experienced by particles which are not in contact with the solvent. An example might be segments inside a collapsed domain of a polymer. There are several other unresolved methodological issues of implicit solvent models which we will not discuss here. A more detailed discussion can be found in review by Hünenberger [23] and references therein.

All simulations in this work were performed using the *ESPResSo* software [24, 25]. It is a versatile simulation package designed mainly for MD simulations of charged soft matter systems in implicit solvent. *ESPResSo* is a continuously developing project, therefore it is futile to describe its contents and functionality. We better refer the reader to its web page [24] which should describe the current status of the project.

Interaction potentials

To correctly define a system, one has to specify the interaction potentials among its particles. Once these are known, the properties of the system can be (at least in principle) calculated using the methods of statistical physics. In this section, we provide a listing of all interaction potentials which are used in various combinations in our simulations. We remind the reader that the polymer models which we use are generic and therefore the choice of the potentials is somewhat arbitrary. A different set of potentials with qualitatively the same features would be expected to yield qualitatively similar results.

The Lennard-Jones potential is our choice to describe the non-bonded Van der Waals type of interactions. In the general form, it is described by the equation

$$U_{\mathrm{LJ}}(r) = \begin{cases} 4\epsilon_{\mathrm{LJ}} \left[\left(\frac{\sigma_{\mathrm{LJ}}}{r - R_{\mathrm{HC}}} \right)^{12} - \left(\frac{\sigma_{\mathrm{LJ}}}{r - R_{\mathrm{HC}}} \right)^{6} + c(R_{\mathrm{c}}) \right] & \text{for } r \leq R_{\mathrm{c}} \\ 0 & \text{for } r \geq R_{\mathrm{c}} \end{cases} , \tag{7}$$

where r is the distance between two particles. The interaction is cut off at a certain distance, R_{c}. In order to make the potential continuous, it is shifted by

$$c(R_{\mathrm{c}}) = (\sigma_{\mathrm{LJ}}/(R_{\mathrm{c}} - R_{\mathrm{HC}}))^6 - (\sigma_{\mathrm{LJ}}/(R_{\mathrm{c}} - R_{\mathrm{HC}}))^{12} , \tag{8}$$

so that it is zero at the end of the interaction range. Other symbols are adjustable parameters of the potential. R_{HC} is the hard-core radius of the particle which is in most cases set to zero. It is the distance from the origin at which the potential diverges.

Several typical special cases of the LJ potential are used in our simulations. If it is not explicitly stated, in all cases we set $R_{\mathrm{HC}} = 0$ and $\sigma_{\mathrm{LJ}} = 1.0$. Because the repulsive part of the LJ potential is rather steep, the value of σ_{LJ} defines the effective size of the monomer unit and it also becomes a very convenient natural unit of length. When we need to account only for the excluded volume interaction, we choose the cutoff radius at the minimum of the potential, i. e. $R_{\mathrm{c}} = 2^{1/6}\,\sigma_{\mathrm{LJ}}$. Together with the shift defined by equation equation (8) the interaction is then purely repulsive. Moreover, it has a continuous first derivative. Such potential is used either for simulations of polymers in athermal solvent or for the interaction of counterions. The properties of the purely repulsive version of the LJ potential do not depend much on the value of ϵ_{LJ} which is for convenience set to $\epsilon_{\mathrm{LJ}} = 1.0$.

Another very common case is when the cutoff radius is set to $R_{\mathrm{c}} = 2.5\,\sigma_{\mathrm{LJ}}$. With such choice of parameters, the potential is strongly repulsive at short distances but at slightly larger distances it passes through a minimum. The exact value of the cutoff is somewhat arbitrary and is chosen so that the potential as well as its first derivative are sufficiently small (almost zero) at $r = R_{\mathrm{c}}$. A typical use of such potential is to simulate a polymer in theta solvent or in a poor solvent. For a polymer in theta solvent, the excluded volume interactions should be compensated by short-range attractive interaction among monomer units so that the chain statistics is ideal (Gaussian). It can be found in literature that this occurs for $\epsilon_{\mathrm{LJ}} = 0.34 \pm 0.02$ [26]. In the case of a polymer in poor solvent, the attractive part prevails, i. e. values of $\epsilon_{\mathrm{LJ}} > 0.34$ are used.

Rather exotic forms of the LJ potential are those when the hard-core radius attains a non-zero value. In the simulations included in this thesis, such situation occurs only in one case. Setting $R_{\mathrm{HC}} \geq 0$ effectively increases the size of the particle while keeping the same depth of the minimum as well as the steepness of the potential walls. This is utilised in the case of central monomer of star polymers where it is desirable to make the central particle slightly larger in order to avoid excessive steric problems when several arms are attached to it.

Besides the Van der Waals type of interactions, chemical bonds exist among the monomers of polymer chains. The bonds are accounted for via a combination of the LJ potential described above with the Finite-extensible nonlinear elastic (FENE) potential. The functional form of the potential is

$$U_{\mathrm{FENE}}(r) = -\frac{1}{2} K_{\mathrm{FENE}} R_{\mathrm{FENE}}^2 \ln\left(1 - \left(\frac{r}{R_{\mathrm{FENE}}}\right)^2\right) . \tag{9}$$

In combination with the LJ potential it forms an anharmonic spring potential. In all our simulations we set $K_{\mathrm{FENE}} = 7.0$ and $R_{\mathrm{FENE}} = 2.0$ which in combination

with our LJ parameters keeps the typical bond length close to 1.0. In contrast to the commonly used harmonic potential, the FENE+LJ spring is stiffer and the separation only has a finite range of allowed values because the combined potential diverges both at R_{HC} and R_{FENE}.

Last but not least, if the simulated system contains charged particles, the electrostatic (Coulomb) interaction is present

$$U_{\mathrm{Coulomb}} = \frac{\lambda_{\mathrm{B}}}{r}\,, \tag{10}$$

where λ_{B} is the is the Bjerrum length defined as

$$\lambda_{\mathrm{B}} = \frac{e^2}{4\pi\varepsilon_0\varepsilon_{\mathrm{r}}k_{\mathrm{B}}T}\,. \tag{11}$$

where e is the elementary charge, k_{B} the Boltzmann constant, ε_0 and ε permittivity of free space and relative permittivity, respectively. The physical meaning of the Bjerrum length is that it is the distance at which the interaction energy of the Coulomb interaction between two charges is equal to $k_{\mathrm{B}}T$. Since all symbols in equation (11) except for temperature are constants (for a particular system), the Bjerrum length nicely fits into the system of reduced units which is used in the simulation.

From the technical point of view, unlike all other interactions, the Coulomb interaction decays very slowly and does not have a definite cutoff distance. Because of these complications, special computational methods have to be used to calculate the electrostatic interactions. These methods are described in the classical textbooks of molecular simulation, such as [17, 18] and we are not going to repeat it in this text. In our work, the particle-particle particle-mesh algorithm [27] for the evaluation of the Ewald sum [28] has been used. It has been implemented in the *ESPResSo* software together with some systematic procedures for setting the parameters of the sum to achieve the desired accuracy [29, 30].

Polymer architectures

The polymers which were simulated in different parts of this work may differ in the parameters of the interaction potentials as well as in topology. They also may or may not contain charged groups. When speaking about polymers in general, by default we mean neutral polymers. If they contain charged groups, they are always

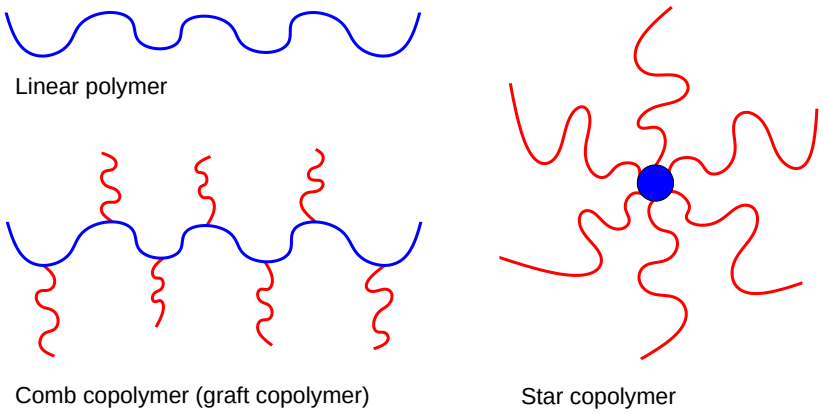

Figure 1. *Schematic illustration of various polymer architectures used in the simulations.*

referred to as polyelectrolytes. Different polymer architectures are schematically shown in Figure 1.

The simplest case is the linear copolymer in which monomer units are arranged in the form of one single chain without any branching points. For such polymer we can set the solvent quality via the Lennard-Jones parameters. For the athermal solvent we set $R_c = 2^{1/6}\sigma_{LJ}$ and $\epsilon_{LJ} = 1.0$. For the poor solvent conditions we set $\epsilon_{LJ} \geq 0.34$ and $R_c = 2.5\sigma_{LJ}$. The solvent can be made poorer by increasing the value of ϵ_{LJ}. As already mentioned in Introduction, we will use the term hydrophobicity as a synonym for solvent quality. Hence, when increasing ϵ_{LJ}, we will speak about decreasing solvent quality for the polymer or increasing hydrophobicity of the polymer.

In polyelectrolyte some of its monomer units are charged. To keep the system electrically neutral, counterions with the opposite charge are present in all polyelectrolyte systems. The counterions interact with all other particles via the repulsive part of the LJ potential, i. e. besides the charge, they also have a finite excluded volume. An important parameter of a polyelectrolyte is its degree of charging, α. It is the fraction of monomer units which are charged. In our simulations charged units are uniformly distributed along the polymer chain, i. e. , if $\alpha = 1/n$, then every n-th monomer unit is charged. A special case is a weak polyelectrolyte, i. e. a polyelectrolyte which contains charged groups whose degree of charging may change in time upon dissociation/association. In such a case we only set the average overall degree of charging and the actual distribution of charges along the polymer backbone is the output of the simulation.

Several linear polymers can be joined to form more complex topologies. These can be random or regular and of several types. In the simulations presented

here, only two regular topologies appear: star and comb-like polymers. Comb-like polymers (also called graft polymers) consist of a backbone to which side-chains (grafts) are attached. If the backbone is only one monomer unit long, we obtain a star polymer. Because only a limited number of side-chains can fit around the single monomer unit of the backbone, in our simulations we make this central monomer unit slightly larger by setting its $R_{\mathrm{HC}} = 3.0$. This corresponds very well to reality as star polymers are often synthesised using rather bulky initiators or coated colloidal particles [2].

If a polymer consists of several different types of monomer units, it is called a copolymer. On the other hand, polyelectrolytes are normally not counted as copolymers if their monomer units only differ by the presence of charge.

Fluorescence anisotropy decays from labelled PE chains

The contents of this chapter are mostly based on the publication „Molecular dynamics simulation of time-resolved fluorescence anisotropy decays from labelled polyelectrolyte chains“ published in *Macromolecules* in 2006 [31]. However, it is not meant to be a mere summary of the already published work. In this text it will be put in a wider context of formation of intramolecular self-organised structures and of our later works in this field. This chapter will also serve as an introduction to pearl-necklace structures in amphiphilic macromolecules which will re-appear in various systems throughout this work.

Time-resolved fluorescence anisotropy

Before discussing the actual simulations related to the topic of this chapter, we have to give an introduction to the experimental methods of time-resolved fluorescence spectroscopy which is the subject of the simulations described in the following paragraphs. Here we only provide a brief description. A more profound discussion of fluorescence methods in general can be found in textbooks such as those by Lakowicz [32, 33]. In context of polymers and their conformational properties the applications of fluorescence methods are discussed in our original paper [31] and in the author's diploma thesis [34] and references therein.

Some molecules, especially aromatic ones, are capable of fluorescence. In this process, a molecule absorbs a photon which brings it to a higher excited state. One of the possibilities is that after a certain period of time (typically on the order of ns) a photon of similar wavelength is emitted by the molecule. The probability of absorption of the photon depends on the mutual orientation of the polarisation of the incident photon and the absorption dipole moment of the molecule. The polarisation of the emission, on the other hand, depends on the orientation of the emission dipole moment of the molecule at the time of emission. Therefore, if polarised light is used for excitation of a sample containing fluorescent molecules (fluorophores), the emitted fluorescence is anisotropic and its anisotropy decays in time due to the rotational diffusion of the fluorophores. In reality, other processes also contribute to the decay [32] but this is beyond the scope of our discussion here. Under certain circumstances they can be neglected which is shortly discussed in the original paper [31]. If the reorientational dynamics of the fluorescent molecule (fluorophore) is on a similar time scale as its fluorescence lifetime, the measurement of the fluorescence anisotropy can be used to monitor its reorientational motion.

The fluorescence anisotropy is defined by the formula

$$r(t) = \frac{I_{\parallel}(t) - I_{\perp}(t)}{I_{\parallel}(t) + 2I_{\perp}(t)}\,, \tag{12}$$

where $I_{\parallel}(t)$ and $I_{\perp}(t)$ are the fluorescence intensities in the direction parallel and perpendicular to the plane of polarisation of the excitation radiation, respectively. $I_{\parallel}(t) + 2I_{\perp}(t)$ is the total fluorescence intensity. There are several theoretical models which describe the fluorescence anisotropy decays of molecules of various complex shapes. An overview of the models is provided in the author's diploma thesis [34] and more detailed information can be found in the book of Lakowicz [32]. Here we only mention that what many models have in common is that the decay can be expressed as a sum of exponential terms

$$r(t) = \sum_i A_i \exp(-t/\tau_i)\,. \tag{13}$$

Here τ_i are individual reorientational relaxation times and A_i are the corresponding pre-exponential factors. In different models, different physical meaning has been assigned to the individual τ_i and A_i values. In practise, however, it is difficult to obtain from experimental data more than two values of the relaxation times with reasonable accuracy. From this point of view, assigning precise physical meaning to the individual relaxation time may be a tricky business. Instead, we can define mean relaxation time τ_{mean} as a weighed average of the individual relaxation times

$$\tau_{\mathrm{mean}} = \frac{\sum_i A_i\tau_i}{\sum_i A_i} = \frac{1}{r(0)}\int_0^{\infty} r(t)dt\,. \tag{14}$$

An obvious advantage is that the mean relaxation time can be computed by numerically integrating the decay curve and thus the ambiguous individual relaxation times and pre-exponential factors can be completely avoided. Comparing the mean relaxation times in the system under different conditions provides the essential information if the reorientational dynamics is slower or faster and yet does not tempt to try to extract more detail from the data than can really be obtained.

It was shown by Szabo [35] that for a fluorophore with a single excited state with orientation-independent radiative rate constant and equilibrium initial orientation distribution the fluorescence anisotropy decay can be calculated from equation:

$$r(t) = \frac{2}{5}\langle P_2[\vec{\mu}_A(0)\cdot\vec{\mu}_E(t)]\rangle\,, \tag{15}$$

where P_2 is the second-order Legendre polynomial, defined by $P_2(x) = \frac{1}{2}(3x^2 - 1)$. Symbols $\vec{\mu}_A(0)$ and $\vec{\mu}_E(t)$ refer to the orientation of the absorption dipole moment at the time of absorption and of the emission dipole moment at the time of emission, respectively. The angular brackets denote ensemble average. This largely simplifies the matters for the simulation because instead of simulating the complicated process of fluorescence which is of quantum origin, to calculate the fluorescence anisotropy decay it is sufficient to calculate the orientational autocorrelation function of the molecule. All other factors such as fluorescence characteristics, mutual orientation of the emission and absorption dipole moments within the molecule, etc. enter equation (15) only as constant prefactors. Therefore they do not interfere with the calculation of the relaxation times and hence can be omitted without loss of generality.

If a fluorophore is chemically attached to a polymer molecule, the motion of the fluorophore will be hindered by the presence of the polymer it is bound to. More specifically, the motion of the fluorophore will be determined by its microenvironment, i. e. by the molecules in its vicinity. In the case of a polymer, one can intuitively distinguish two extreme cases of such behaviour. The first one occurs when the solvent is poor for the polymer which then adopts a compact globular conformation. In such case, the microenvironment of the fluorophore attached to the polymer strongly hinders its motion and slows down its reorientational dynamics. This, in turn, results in a slow decay of the fluorescence anisotropy, i. e. long reorientational relaxation time of the fluorophore. On the other hand, if the solvent is good for the polymer, it adopts a loose Gaussian-coil conformation which provides much smaller hindrance for the motion of the fluorophore. In such case the fluorescence anisotropy decay is fast, i. e. the relaxation time is short. It is also important that the fluorescence anisotropy decay only gives us information about the local conformation in the vicinity of the fluorescent label.

The measurement of fluorescence anisotropy decays described above provides only indirect information about the conformational changes of the polymer. Though it may be anticipated that the above description is correct, it remains a hypothesis if unsupported by some independent argument. One way to provide an independent supporting evidence is to perform a molecular simulation of such system and to analyse the data in the same way as it is done in the experiment. One such experimental study has been performed in our lab by Bednář et al. [36] about 20 years ago. They were following the change of behaviour of poly(methacrylic acid) (PMA) upon change in pH. Since PMA is a weak polyacid, it was expected that it would expand upon a decrease in pH, as its degree of charging would increase. The authors observed this change via the measurement of fluorescence anisotropy decays from a fluorescent label attached to the polymer chain. By that time the interpretation of the indirect fluorescence anisotropy ex-

periments was based mainly on the authors' intuition. Supporting evidence for their interpretation came in 2006 in our publication [31].

Results and discussion

For the purpose of this study, we have simulated a series of linear polyelectrolytes with a pendant fluorescent label attached as a short side-chain. They structure of a section of such polymer and the attached fluorescent label is schematically shown in Figure 2. A series of polymers in a range of solvent quality conditions and degrees of charging was simulated. The parameters of the simulated polymers are listed in Table 1.

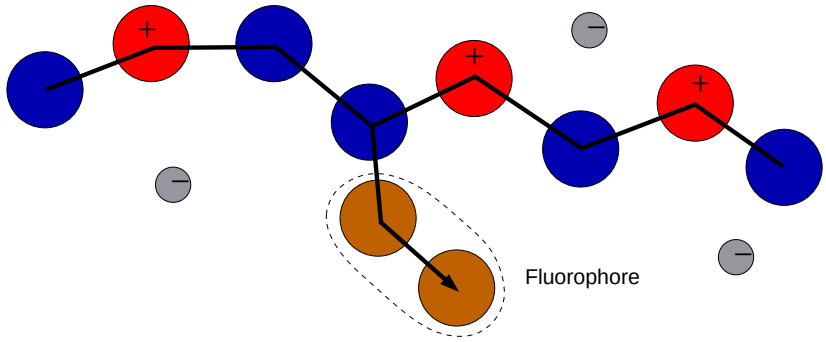

Figure 2. *Schematic illustration of the polymer model used for the simulation of fluorescence anisotropy decays.*

Chain length	Degree of charging	ϵ_{LJ} (solvent quality)
200	0.06–0.5	1.0
200	0.06–0.5	1.3
200	0.06–0.5	1.6
200	0.06–0.5	2.0

Table 1. *Parameters of the simulated polymers*

The simulation results have shown that polyelectrolytes in poor solvents form pearl-necklace conformations in a certain range of conditions. This finding was not really new as it had been predicted by theory [8] and confirmed by computer simulations [9, 10] before our data were published. Nevertheless, for ease of reference we show here a series of simulation snapshots which illustrate the observed

behaviour. Figure 3 shows typical conformation of the polyelectrolyte in rather poor solvent ($\epsilon_{\mathrm{LJ}} = 1.3$) for several different degrees of dissociation, α. Starting from the left at $\alpha = 0.06$ the polymer adopts globular conformation. At a slightly higher value of $\alpha = 0.20$ the polymer globule is deformed and at even higher degree of charging, $\alpha = 0.25$ it splits into two pearls. Finally, when α exceeds a certain threshold, the pearls disappear as shown for $\alpha = 0.33$. This observation is in line with theoretical predictions [8] as well as earlier simulations by other authors [9, 10] which also contain a more detailed analysis of the structures and conditions under which they are formed.

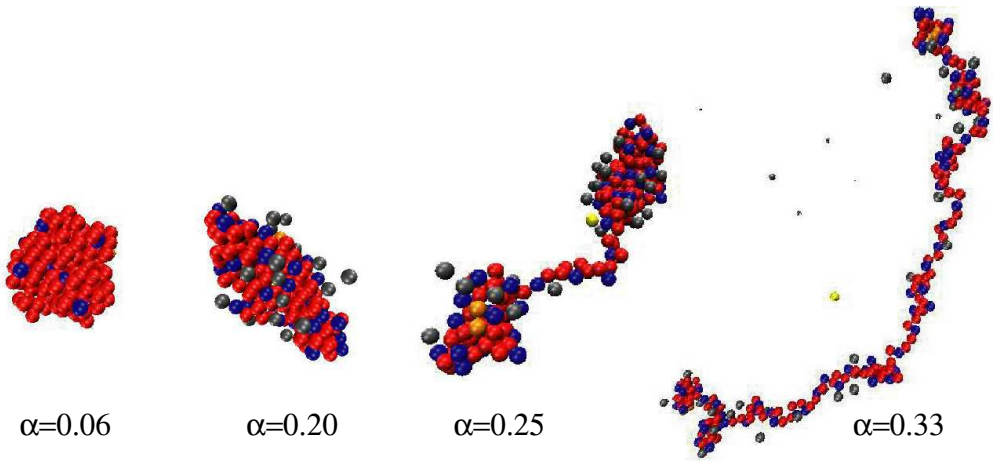

Figure 3. *Simulation snapshots of polyelectrolyte in poor solvent ($\epsilon_{\mathrm{LJ}} = 1.3$) at various degrees of charging, α as indicated in the figure.*

What was new in our work in contrast with the earlier theoretical and simulation studies, was the comparison of the simulation results with the earlier experimental data on measurements of fluorescence anisotropy decays from labelled PMA chains [36]. In particular, we have confirmed the anticipated relation between the mean orientational relaxation time of the fluorophore attached to the polymer, τ_{mean}, and the conformational changes due to the varying degree of charging. To establish this relation, in Figure 4 we show the comparison of the simulated and experimentally observed variation of τ_{mean} with the degree of charging of the polymer.

Because we were using a generic polymer model with a number of adjustable parameters, we could not expect more than a semi-quantitative agreement. In the experimental study which was used for comparison [36] the dependence of the reorientational relaxation times on pH was measured for samples of poly(methacrylic acid). To compare the data it was necessary to convert the pH-scale to the degree

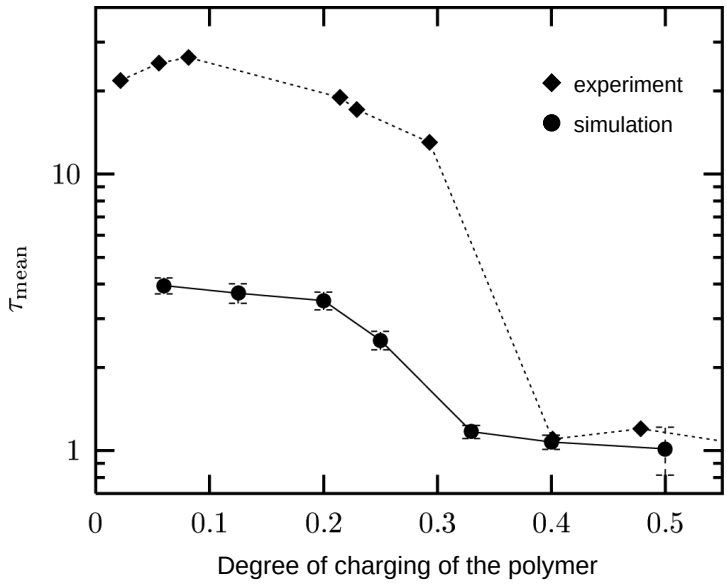

Figure 4. *Comparison of the simulated mean relaxation times and experimental data as a function of the degree of dissociation of the polyelectrolyte. The experimental data on poly(methacrylic acid) are taken from Ref. [31].*

of dissociation. For this purpose we used the measured values of the effective acidity constant of PMA on pH [37]. For the comparison, we chose the polymer with $\epsilon_{\mathrm{LJ}} = 1.3$ because its conformational transition was in the same range of degrees of dissociation.

The conversion of the reduced time units from the simulation into the real units of ns was done using the mapping when one monomer unit of the generic model would correspond to one unit of the real polymer. However, the mapping is not uniquely defined and this choice is arbitrary to a certain extent. Hence, the conversion is correct up to an unknown multiplicative pre-factor (presumably of the order of 1.0–10.0). Considering the above-mentioned caveats, we can argue that on a semi-quantitative level the two curves in Figure 4 agree. Therefore, the simulations confirm the intuitively expected relation between the conformational changes of the polymer and the reorientational relaxation times of the fluorescent label attached to it.

As it often happens in research, apart from providing answers to some old unresolved problems, our simulation study of fluorescence anisotropy decays has open a series of new questions. An important caveat of the whole comparison was the fact that we used a polyelectrolyte with a pre-defined degree of dissociation and uniform distribution of charged units along the polymer chain while in the real experiment, PMA is a weak polyelectrolyte whose degree of dissociation is deter-

mined by the solution pH. From some theoretical works it was known that certain ranges of degree of dissociation might be forbidden for weak polyelectrolytes in poor solvents [38]. Even though other simulation studies [39–42] suggested that this may not always be the case, it was clear that it would be desirable to simulate a weak polyelectrolyte rather than a strong one. By the time of the publication of our simulations of the anisotropy decays [31], weak polyelectrolytes could be simulated using the semi-grandcanonical Monte Carlo (GCMC) techniques but no appropriate model had been developed for the MD simulation method. In the following years we devoted a significant part of our efforts to development of such models. This development is still in progress and some of its results are the subject of the last chapter of this dissertation.

Comb copolymers in selective solvents

This chapter is based on our two publications concerning comb-like copolymers. Both were motivated by the scaling analysis of of intramolecular conformational transitions in comb-like copolymers in selective solvents which was published by Borisov and Zhulina in 2005 [11].

Scaling theory of comb copolymers in selective solvents

We begin with a brief summary of the main qualitative conclusions of the above-mentioned scaling theory with which we will compare the simulations. Borisov and Zhulina have considered a neutral comb-like copolymer in selective solvent which is poor for the backbone and at the same time good for the side-chains. Such polymer is schematically depicted in Figure 5.

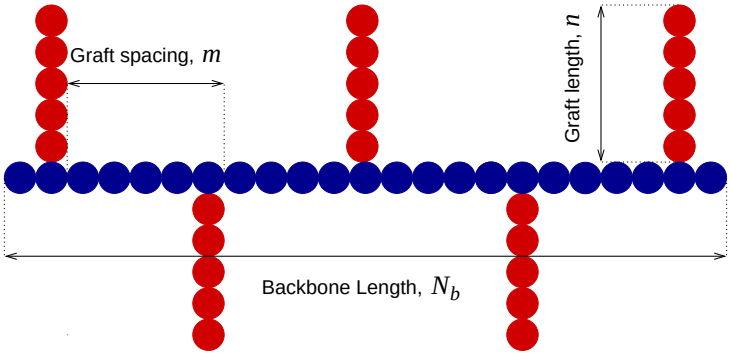

Figure 5. *Schematic illustration of the architecture comb-like copolymer. Blue – backbone, red – side-chains.*

Because the solvent is poor for the backbone, the backbone has tendency to collapse and form a compact globular structure. On the other hand, the steric repulsion of the side-chains counteracts the collapse. Equilibrium is attained when the two forces exactly counterbalance each other. This situation is in certain aspects analogous to the formation of pearl-necklace structures in linear polyelectrolytes which was described in the previous chapter. The important difference, however, is that the force which brings about the expansion is of different origin and hence controlled by other parameters than in the case of the polyelectrolytes. In other aspects, the behaviour of this system is analogous to the block-copolymer micelles, where the core composed of poorly soluble blocks is stabilised by the steric repulsion within the corona formed by the well soluble blocks.

If the backbone is in a theta-solvent, the comb copolymer adopts a bottlebrush

structure. The steric repulsion among the side-chains causes that the bottlebrush has an induced persistence length which is larger than that of the backbone alone. This had already been found by Birshtein et al. [43].

For the backbone in poor solvent the scaling theory distinguishes two main regimes according to the value of the grafting density parameter

$$\zeta = \frac{n^{3/5} v^{1/5}}{m^{1/2}}\,, \tag{16}$$

where symbols n and m refer to the length of the side-chains and spacing between them, respectively, as illustrated in Figure 5. Parameter v is the excluded-volume of the monomer unit, (the second virial coefficient normalised by the cube of the monomer unit length) and its value is of the order of unity, $v \approx 1$.

The densely grafted regime is realised when $\zeta \gg 1$. Since $v \approx 1$, this condition is usually fulfilled when $n \gg m$. The theory anticipated that in the densely grafted regime the backbone of the comb copolymer forms a pearl-necklace structure. Because the pearls are analogous to block copolymer micelles, they are also referred to as intramolecular micelles with the corona formed by the side-chains. The size of the micelles is controlled by the grafting density as well as by the quality of solvent for the backbone (backbone hydrophobicity). According to the original version of the theory, the pearls appear discontinuously after a certain threshold in the solvent quality is reached. For a polymer of a given architecture, the size of the pearls then increases with decreasing solvent quality for the backbone. Since the total number of monomer units in the backbone, N_{B}, is fixed, an increase in the size of the pearls implies a decrease in their number. This continues until the whole molecule ends up in a single intramolecular micelle.

The regime when $\zeta \ll 1$ is called sparsely grafted. In analogy with the previous case, because $v \approx 1$, the sparsely grafted regime is usually realised when $m \geq n$. Upon a decrease in solvent quality for the backbone, polymer in this regime was also anticipated to go through a series of pearl-necklace conformations similar to the previous case. However, the final state is not a spherical micelle but a cylindrical one.

Apart from the two regimes with intramolecular micelles which were described in the previous paragraphs, the scaling theory predicted also regimes where phase separation may occur or where lamellar structures are formed. We will not discuss them in detail here because due to technical limitations it was not possible to study them using our simulation techniques. If the reader is interested in other regimes, we refer him to the original paper by Borisov and Zhulina [11].

Simulations of neutral combs in selective solvents

This part of the chapter deals with neutral copolymers in selective solvents. The results presented here are largely contained in our publication in Macromolecules [12] which was produced in cooperation with Oleg Borisov and Ekaterina Zhulina. This paper consists of two parts. The MD simulations were performed bu ourselves and the augmented scaling theory was developed by our collaborators. The interpretation of the results is the product of collaborative effort of the whole team.

One might want to ask the question why it was useful to perform extensive simulations if the matter had already been treated by a theoretical model. It is hidden in the way this theoretical model was developed: it compared free energies of anticipated structures and then found out which corresponds to the global minimum of free energy. However, there is no procedure other than simulations which could be used to obtain these structures from first principles. Instead, in the course of development of the theory one has to rely on intuition or analogy with known systems. Therefore it is desirable to verify that the predicted structures are the correct ones and one of the ways to do so is to perform molecular simulations.

backbone length N_B	side-chain length n	side-chain spacing m	backbone hydrophobicity ϵ_{LJ}
320	40	4	0.3–2.0
320	40	8	0.3–1.4
320	5	4	0.6–1.5
320	5	6	0.6–1.5
320	5	8	0.6–1.5
500	5	6	1.2

Table 2. *Architectures of simulated copolymers. The backbone length, N_B, is the same for all systems except one. Two values of side-chain length, n, are used and for each of them a series of spacings, m. The horizontal line separates the systems with high (top) and low (bottom) grafting densities.*

The polymers we simulated consisted of a backbone for which the solvent was poor. Side-chains for which the solvent was athermal were attached to the backbone. We simulated two series of polymers – densely and sparsely grafted. In each of these regimes, we simulated a few polymers with different grafting densities and each of these polymers was simulated in a range of solvent qualities for the back-

bone, starting from close-to-theta and ending up in a very poor solvent. Because the grafting density parameter is a function of both the side-chain length, n, and spacing, m, we varied the grafting density in such a way that for each regime we chose a fixed length of the side-chains and then we only varied the spacing between them. The parameters of the simulated polymers are listed in Table 2.

The simulation results qualitatively confirmed the predictions of the scaling theory concerning the types of structures which are formed in the two regimes and the trends in the number and size of intramolecular micelles. We did not attempt to verify the scaling exponents as this would require to perform a series of simulations where the variables comprising the scaling parameters would differ by at least one order of magnitude. This would require too large polymers and consequently unacceptably long simulation times. Even some of our current simulations required about one month of computer time.

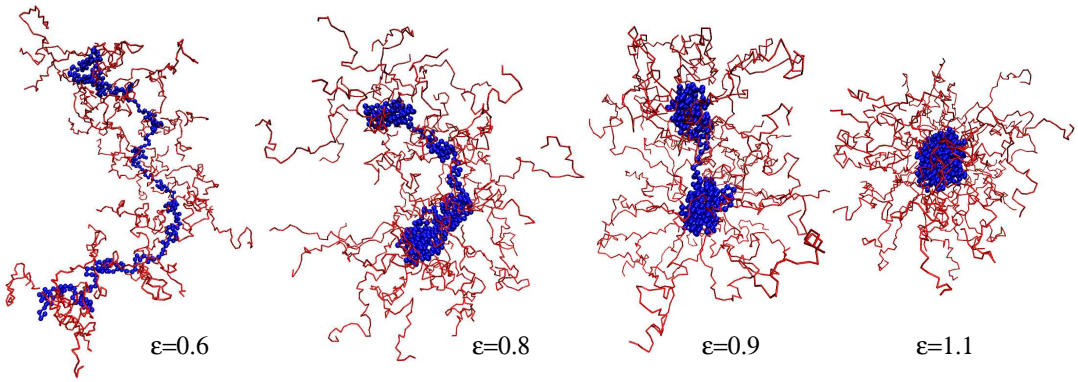

Figure 6. *Simulation snapshots of the copolymers with high grafting density with the graft spacing $m = 8$. For other parameters see Table 2. For better visibility, the side-chains are only rendered as thin lines and magnification slightly increases from left to right.*

To illustrate the qualitative agreement with the theory, we show two series of simulation snapshots. In Figure 6 we show the simulation snapshots of a polymer with high grafting density ($m = 8$) for several values of hydrophobicity of the backbone as indicated in the figure. For $\epsilon_{\mathrm{LJ}} = 0.6$ (relatively close to theta state) no significant formation of pearls is observed. Upon an increase in ϵ_{LJ} we can observe formation of three and later two pearls and finally at $\epsilon_{\mathrm{LJ}} \geq 1.1$ the system ends up in a single spherical intramolecular micelle. In Figure 7 a similar series of snapshots is shown for a sparsely grafted polymer ($m = 6$). Again we can observe a transition from a relatively stretched conformation with no pearls through pearl-

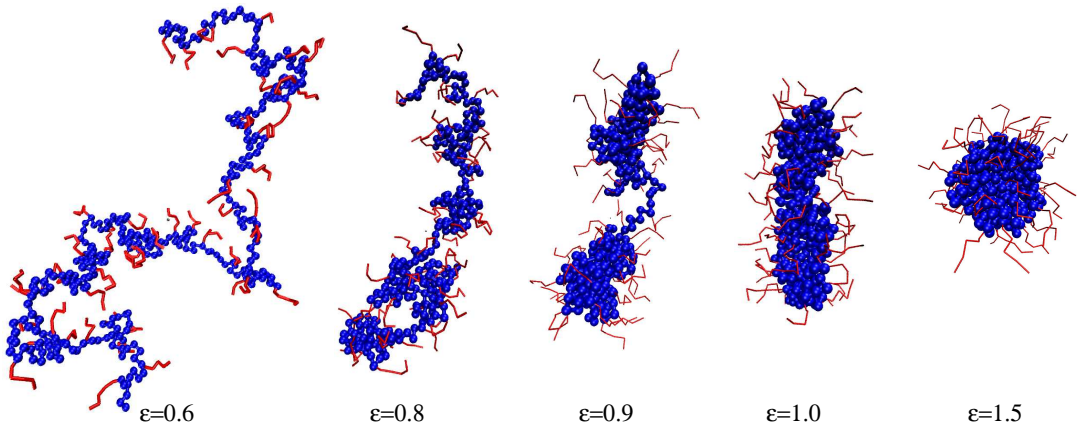

Figure 7. *Simulation snapshots of the copolymers with low grafting density with the graft spacing $m = 6$. For other parameters see Table 2. For better visibility, the side-chains are only rendered as thin lines and magnification slightly increases from left to right.*

necklace up to a cylindrical micelle and finally to a spherical micelle. Apart from the very last snapshot, everything else is in agreement with the predictions of the theory.

A more quantitative view of the conformational changes can be obtained by explicitly counting the number of pearls and calculating the corresponding averages. The counting was performed using the algorithm developed by Limbach et al. [9]. Figure 8 shows the number of pearls in copolymers with high grafting density as a function of hydrophobicity of the backbone for two different values of spacing between the grafts. In both cases we can observe first a gradual growth of the number of pearls with increasing ϵ_{LJ}. After the number of pearls passes through a maximum, it decreases again and levels off at a constant value. For $m = 8$ it levels off at one pearl while for $m = 4$ it levels off at two pearls. It can be noticed that the plot of the number of pearls contains certain features which were not predicted by the original version of the theory. Yet these features have a clear explanation and from the explanation it can also be understood why the original theory failed to predict them.

We begin with the gradual increase in the number of pearls in contrast with the discontinuous increase predicted by the theory. The problem is that the scaling theory predicted only the global free energy minimum for the limit of infinitely long chain. In other words, this approach completely neglected fluctuations which may be very important in finite-sized systems, especially around the transition point. And indeed in our systems, especially on the left from maximum of the number of pearls, fluctuations play an important role. This can be seen either from the

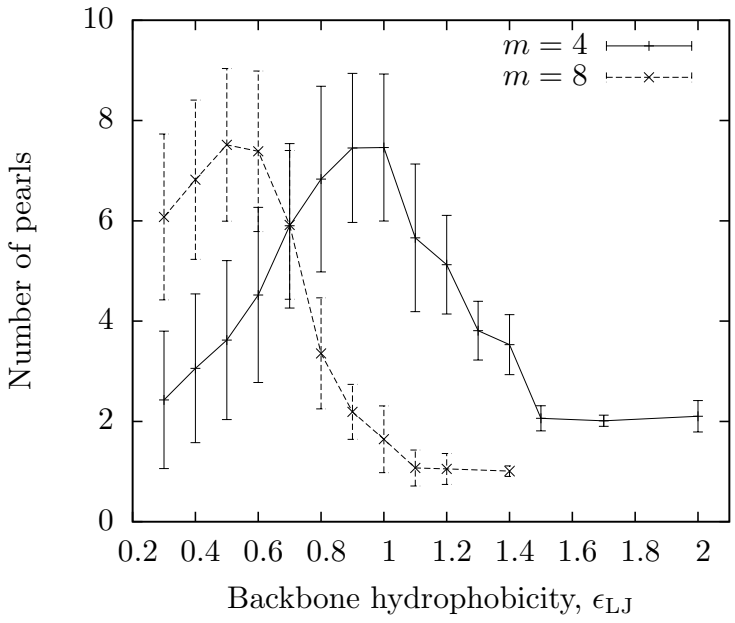

Figure 8. *Number of pearls as a function of solvent quality for the backbone for the polymers with high grafting density.*

size of the error bars which are much larger on the left from the maximum than on the right, or from a simulation movie which shows that pearls appear and disappear repeatedly during the simulation run [44]. It indicates that the free energy landscape has several minima of comparable depth which are separated by low barriers. Upon an increase in ϵ_{LJ}, the relative depth of the minima increases, enthalpy wins over entropy and pearls become stable which is manifested by a systematic decrease of the size of the error bars on the right from the maximum of the curves in Figure 8.

Another issue is the very poor solvent limit in which some systems end up in a state with two pearls rather than one pearl which was predicted by the theory. It can be understood by an analogy with surfactant or block copolymer micelles. Their aggregation number grows until a certain threshold is reached, beyond which the hydrophobic chains are not able to fill the core effectively. This maximum size of the micelle is, for a fixed length of the hydrophilic block, given by the length of the hydrophobic one. The same is observed in the case of intramolecular micelles which grow until a certain maximum size which is primarily determined by the length of the spacer between the side-chains. If the whole backbone is smaller than or comparable to this maximum pearl size then in very poor solvent the polymer forms a single intramolecular micelle. On the other hand, if the backbone is much larger than the maximum pearl size, then in the poor solvent the polymer ends up in a pearl-necklace structure composed of pearls which have the maximum size. It

is noteworthy that in principle, the maximum pearl size could have been predicted by the original theory. The main reason why it was not predicted was that it was not anticipated before it was observed in simulations.

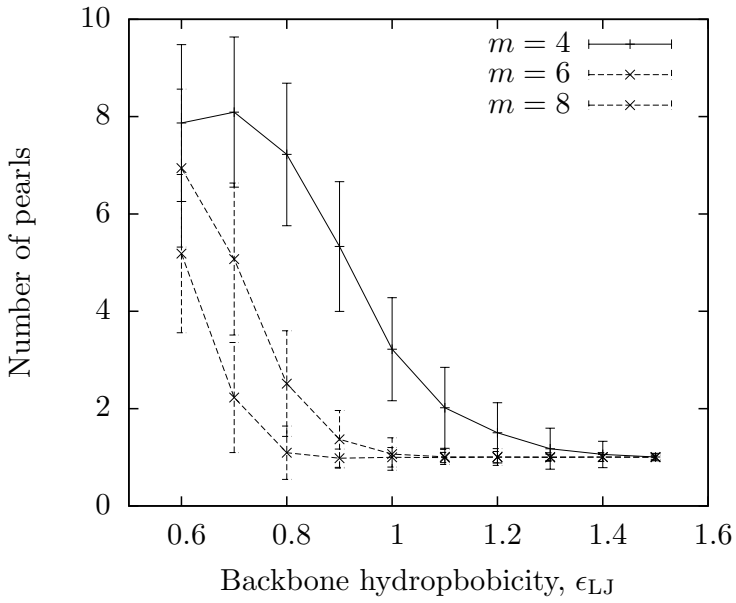

Figure 9. *Number of pearls as a function of solvent quality for the backbone for the polymers with low grafting density.*

A similar problem with the maximum size appears in a slightly different perspective in the case of copolymers with low grafting density. In this case the original theory predicted the formation of cylindrical micelles as the limiting state under very poor solvent conditions for the backbone. From the plot of the number of pearls in Figure 9 we can see that in this case all systems end up in a single intramolecular aggregate. To analyse the shape of the aggregate, we can determine its asphericity [45] which has the property that it is zero for a spherical object and attains positive values for other shapes which deviate from the spherical symmetry. From the plot of the asphericities of the backbones, A_{d}, shown in Figure 10 we can see that some of them become eventually spherical ($A_{\mathrm{d}} = 0$) at high ϵ_{LJ} while those with short spacers between the side-chains retain roughly the same asphericity for all values of ϵ_{LJ}. More detailed discussion of the asphericities can be found in the original paper [12]. Here we only summarise the conclusions. While in the case of the pearl-necklace we found the maximum pearl size, in the case of cylindrical micelles we analogically find the maximum radius of the cylinder. If the backbone is large enough so that the length of the cylinder is significantly larger than its maximum radius, cylindrical micelles are formed. On the other hand, if

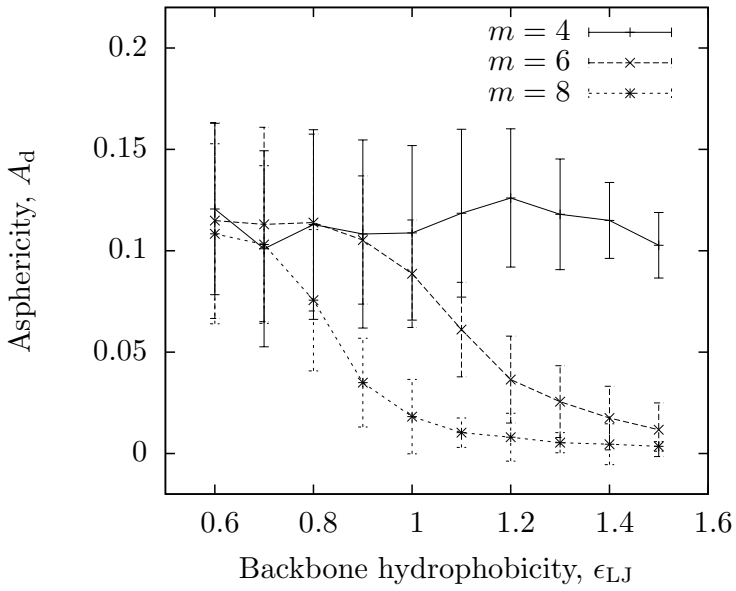

Figure 10. *Asphericity of conformation as a function of solvent quality for the backbone for the polymers with low grafting density.*

the backbone is not large enough and the length of the cylinder is comparable to its width spherical micelles are formed.

The results of MD simulations of comb copolymers in selective solvents and the augmented scaling theory can be summarised in a quasi phase diagram shown in Figure 11. In contrast to the phase diagram published in the original paper by Borisov and Zhulina [11] it does not contain regions which were not explored in our simulations but within the explored part of the conformational space it contains certain new features. In the poor solvent region close to the theta conditions for the backbone there is a region of pearl nucleation. In this region fluctuations play an important role and the polymer conformation cannot be represented by any typical shape. It is noteworthy that the boundaries of the nucleation zone are not sharp but diffuse. Further in the poor solvent there comes a region of stable pearl-necklace conformations (intramolecular micelles). Finally, in very poor solvents the densely grafted copolymers end up in a chain of intramolecular micelles of maximum pearl size while the sparsely grafted copolymers end up in a single cylindrical micelle. If the backbone of the polymer is not long enough then the limiting state is a single spherical micelle.

Comb polyelectrolytes in selective solvents

The results presented in this section have been published in 2007 in Journal of Physical Chemistry [13]. The simulation study of comb-like polyelectrolytes

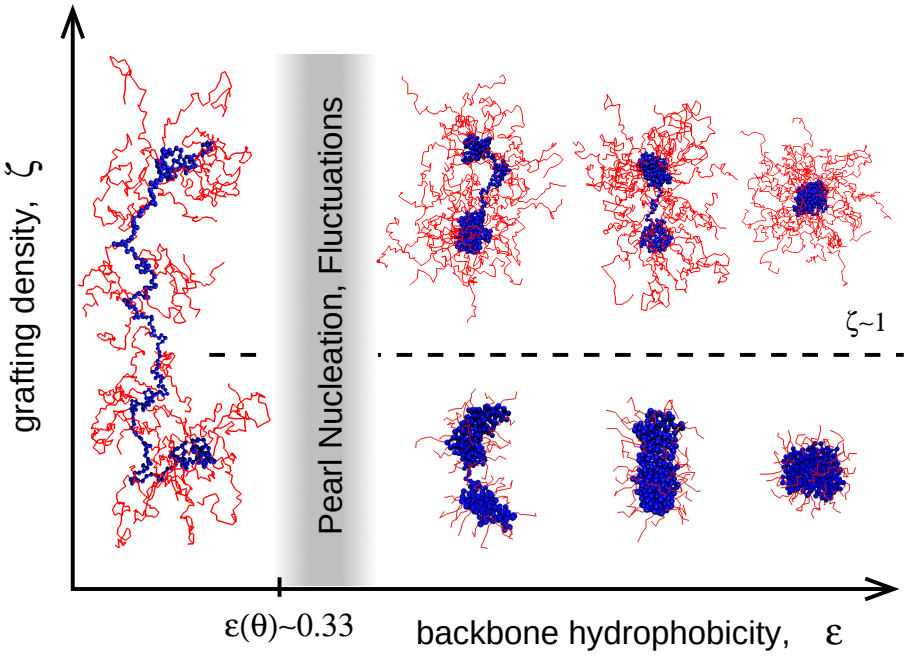

Figure 11. *Schematic phase diagram showing different conformations of comb copolymers in selective solvents. The horizontal line $\zeta = 1$ separates the polymers with high ($\zeta > 1$) and low ($\zeta < 1$) grafting density. The spherical structures in the very poor solvent regime are attained only for short backbones. The grey region with diffuse boundaries is dominated by fluctuations. In this region the polymer cannot be represented by a typical well-defined structure.*

was motivated by the publication of the theoretical paper on the behaviour of neutral comb copolymers by Borisov and Zhulina [11]. We anticipated that comb-like polyelectrolytes could exhibit behaviour similar to the one predicted for the neutral polymers, namely the formation of the pearl-necklace structures in the backbone. Historically these simulations were performed and published before we started more intensive cooperation with the Russian theoreticians. Besides summarising the simulation results which are much alike the ones from the previous section, we will point out some specific features which are more pronounced in the polyelectrolyte case because of the long-range nature of the electrostatic interactions.

The underlying mechanism of the formation of the intramolecular structures in the comb-like polyelectrolytes is similar to the case of the neutral combs. However, the principal difference is that in the polyelectrolyte case the repulsion among the side-chains is of electrostatic origin. Therefore, apart from structural parameters, the strength of the electrostatic interaction is important. It is determined by the

degree of charging of the polyelectrolyte side-chains, the Bjerrum length and the ionic strength of the solution.

The polymers we simulated in this study consist of a hydrophobic backbone to which polyelectrolyte side-chains are attached. For the interaction among the monomer units of the backbone we set $\epsilon_{\mathrm{LJ}} = 2.0$ which corresponds to very poor solvent. For the side-chain – side-chain interaction we set $\epsilon_{\mathrm{LJ}} = 0.4$ which is close to theta solvent when the side-chains are neutral. However, when they are charged, they exhibit strong stretching. For the backbone – side-chain interaction we set $\epsilon_{\mathrm{LJ}} = 0.89$ which is the geometric mean of the previous two.

identification	number of side-chains	side-chain length	backbone length
10×60	10	60	240
30×20	30	20	240
60×10	60	10	240

Table 3. *Architectures of simulated comb-like polyelectrolytes. The backbone length, N_{B}, is the same for all systems. The values of side-chain length, n, and their length are chosen so that the total number of monomer units in the side-chains is constant.*

We have systematically varied the number and length of the side-chains so that the total number of monomer units in the side-chains was kept constant. Each of these polymers was simulated in a range of degrees of dissociation 0.125 – 0.50. The structural parameters of the simulated comb-like polyelectrolytes are summarised in Table 3. In further text we will refer to different polymer architectures as *(number of side-chains* $\times$ *side-chain length)* as indicated in the first column of Table 3. We did not employ the same strategy as in the case of the neutral combs because in the polyelectrolyte case the mere grafting density is not the key control parameter. One could possibly define some effective grafting density which would include the degree of charging within a theoretical framework for the description of the comb-like polyelectrolytes, however, at the time of writing this thesis, no such theory has been formulated.

To envision the pearl-necklace structure on the backbone of the polymers, in our study of comb-like polyelectrolytes we used the bond angles between consecutive bonds along the backbone as the variable for local conformational analysis. We define the average bond angle cosine, $\cos(\theta_i)$, as the normalised scalar product of

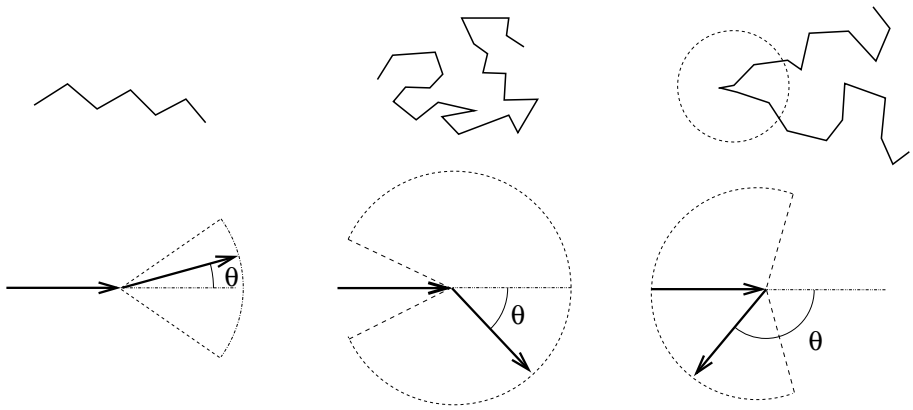

Figure 12. *Schematic illustration of the typical values of the bond angles for various local conformations. On the left, a stretched part of the chain is depicted. In such conformation, the bond angle is restricted to small values as indicated in the scheme below. In the middle, a random conformation is shown where the bond angle can attain almost any value. On the right, a loop in the chain is shown. In such case the bond angle attains preferentially values larger than* $\pi/2$.

consecutive bond vectors

$$\langle \cos(\theta_i) \rangle = \langle \vec{r}_i \cdot \vec{r}_{i+1} \rangle \ , \tag{17}$$

where $\vec{r}_i$ is the bond vector between the i-th and $(i+1)$-st monomer unit. Both vectors are normalised to unit length. The angular brackets denote averaging over all polymer conformations. For a part of the polymer chain which is stretched, the bond angle θ is restricted to values close to zero, as indicated in Figure 12. Consequently, the value of $\langle \cos(\theta_i) \rangle$ is close to 1.0. On the other hand, in a collapsed domain, the bond angle with equal probability attains all values except the ones close to π due to the excluded volume, resulting in $\langle \cos(\theta_i) \rangle \approx 0$. In an extreme case when the chain loops back, the angle θ mostly attains values larger than $\pi/2$ which results in negative values of $\langle \cos(\theta_i) \rangle$. All these situations are schematically shown in Figure 12.

Plots of the average bond angle cosines are shown in Figure 13 for three different polymer architectures and degrees of charging of the side-chains. The plots for the 10×60 architecture contain only values close to zero and are otherwise featureless which indicates that the backbone contains one single domain. This is in agreement with the corresponding simulation snapshots presented in Figure 14 which show a micelle-like structure for the 10×60 system at all degrees of charging. For the polymer with more grafts of shorter length, 30×20, the plots for higher degrees of charging, $\alpha \geq 0.33$, have a peak in the middle which indicates that the central part of the backbone is strongly stretched while the ends are collapses into pearls.

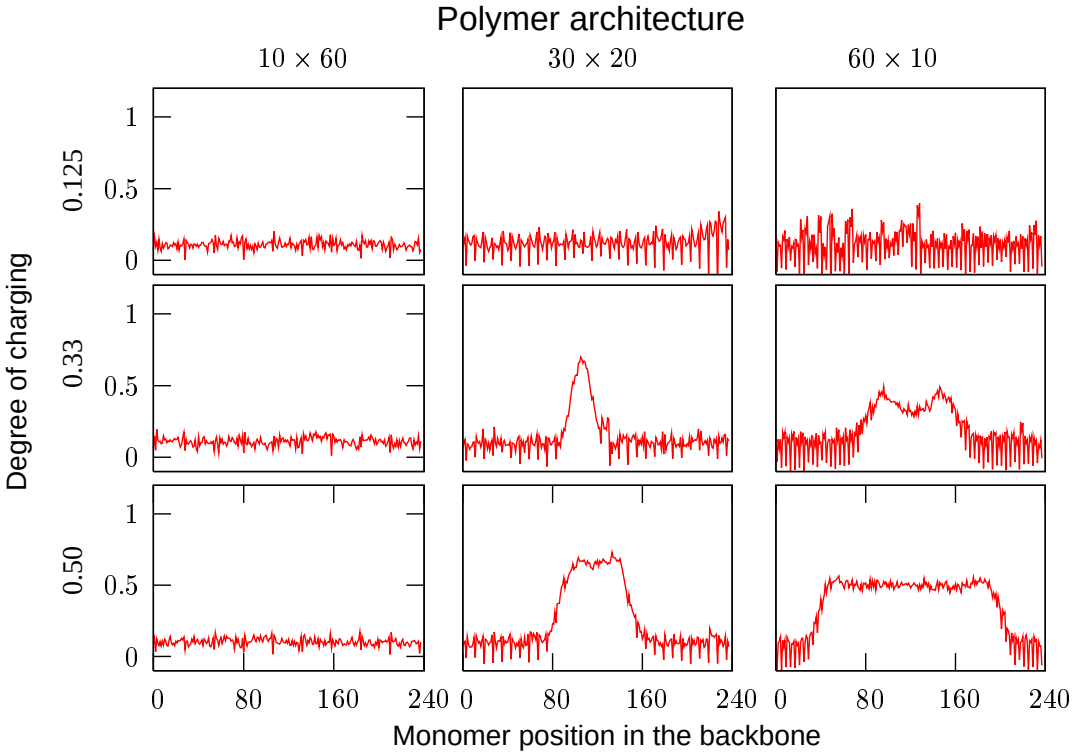

Figure 13. *Plots of the average cosine of the bond angles, $\langle\cos(\theta_i)\rangle$, as a function of position in the backbone.*

Again, this is in agreement with the corresponding simulation snapshots shown in Figure 14. The situation is very similar in the 60×10 system shown in the last column of both above-mentioned figures but the stretching of the central part is even more pronounced. At $\alpha = 0.33$ we can also observe a local minimum in the middle. This is a signature of a third pearl which is smaller than the two at the ends. The snapshots in Figure 14 once again confirm the interpretation of the plots of the bond angles.

The plots of the bond angle cosines contain more information than discussed above. They also show that the internal structure of the pearls is not random but organised. To envision this organisation, in Figure 15 we show a magnification of parts of selected plots from Figure 13. We can see that what might have seemed as noise in Figure 13 is actually a fine structure of the plot with negative spikes at regular intervals. The positions of the spikes correspond to the grafting points on the backbone where side-chains are attached. The negative values of $\langle\cos(\theta_i)\rangle$ mean that at the grafting points bond angles larger than $\pi/2$ prevail, i. e. the chain forms a loop. It can be explained when we realise that the grafting point is being pulled out of the pearl by the polyelectrolyte side-chain. Therefore, the grafting

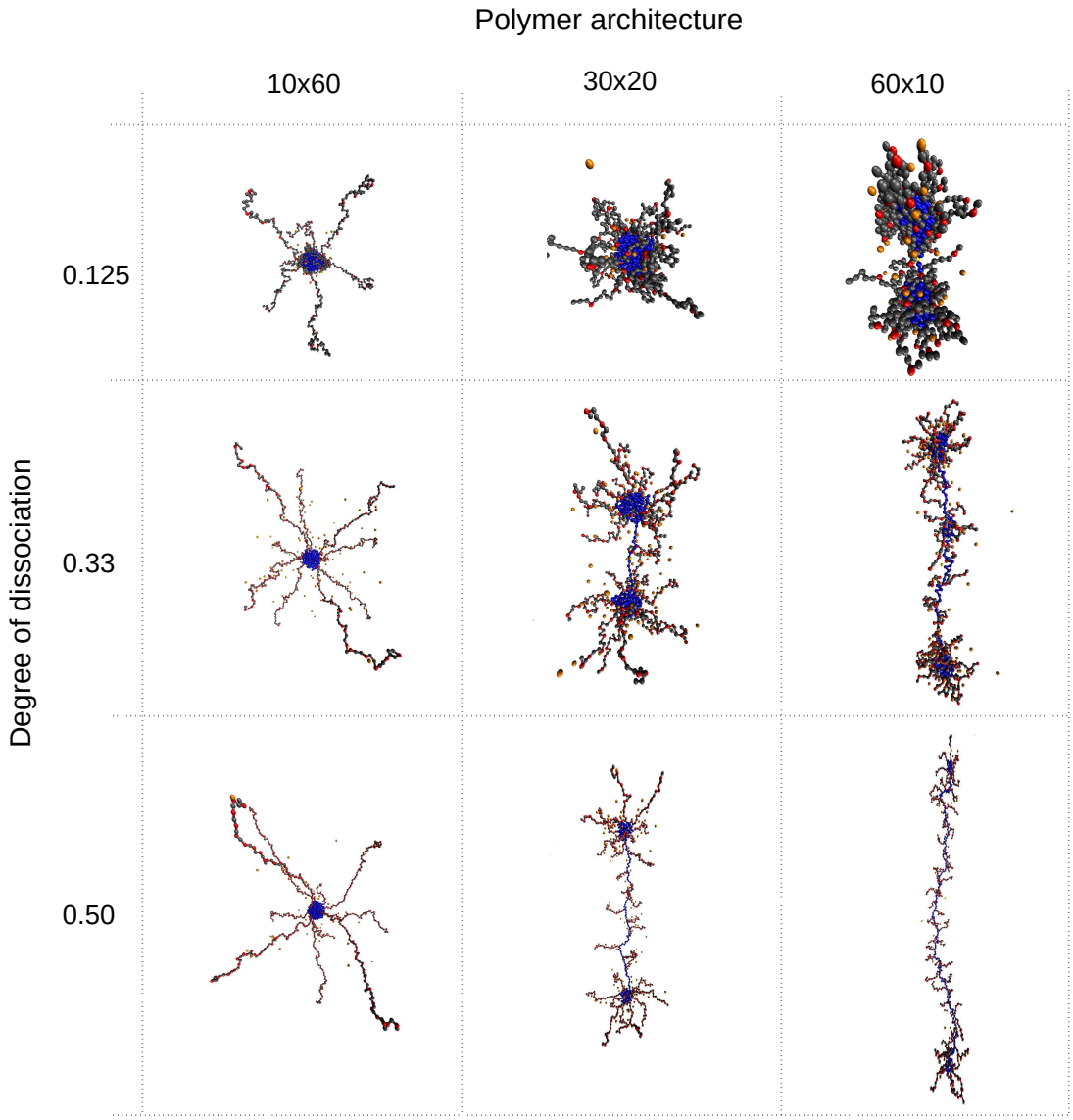

Figure 14. *Simulation snapshots of comb-like polyelectrolytes. For better visibility, magnification of different snapshots slightly increases from left to right and from bottom to top. Backbone: blue, Side-chains: red-charged, grey-uncharged, Counterions: orange.*

points are preferentially localised at the surface of the pearls while the interior is preferentially filled by the intermediate segments of the backbone (those between the grafting points). Knowing that the maximum size of the pearl is approximately one half of the length of the spacer, we may argue that as the radius of the pearl approaches this value, its internal structure becomes increasingly organised. The stretching and alignment of the spacers increases as it becomes more and more difficult to satisfy the constraint that the branch points want to be close to

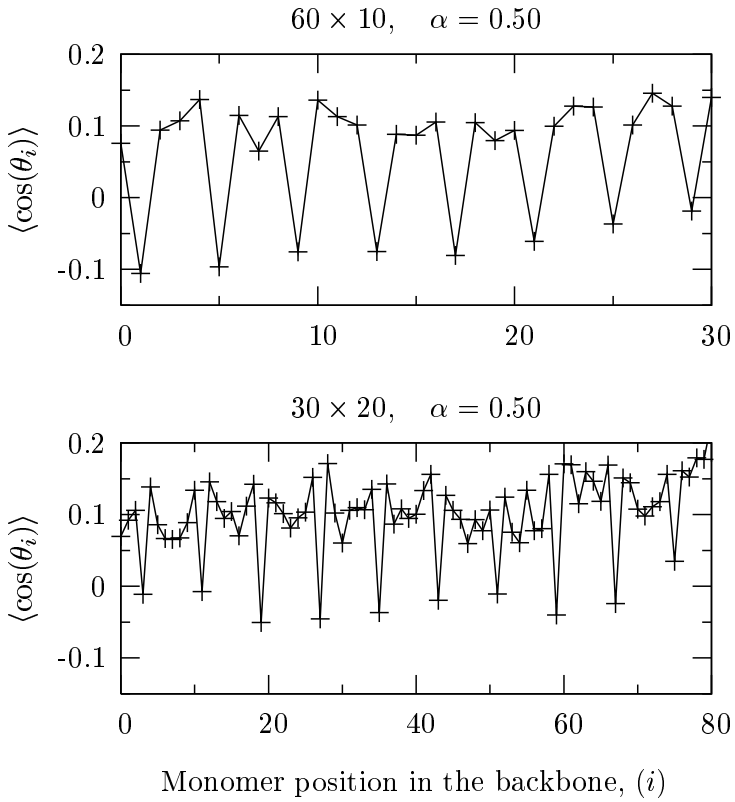

Figure 15. *Magnification of parts of selected plots from Figure 13. Fine structure with negative spikes at regular intervals is visible.*

the surface and the intermediate segments have to fill the interior. This induced alignment of the spacers might in a real polymer induce crystallisation within the collapsed domains. It would be very interesting to explore this effect but unfortunately it is beyond the abilities of the polymer model we used.

It should be noted that in principle similar plots can be obtained for the neutral graft copolymers and more generally for any polymers forming pearl-necklace structures. However, only in the case of the comb-like polyelectrolytes they have well-defined structure and even observable fine structure. Similar plots for the neutral combs have been published in our paper [12] but the desired features are almost buried in the noise. To reduce the noise one would have to perform extremely long simulations lasting a couple of months on contemporary computers. The reason why the plots of the neutral polymers are much more noisy is the different nature and range of the repulsive interaction among the side-chains. The steric repulsion in the corona of the neutral combs has got a range on the order of the radius of gyration of the side-chains which means it is a local interaction. On the other hand, the electrostatic repulsion in the corona of the comb-like polyelectrolyte is long-ranged. Therefore, every pair of equally charged particles in the

corona contributes to the repulsive interaction which keeps the spacers strongly stretched and the pearls in a fixed position.

To conclude the chapter on comb-like polymers we can say that both the neutral and polyelectrolyte combs can form self-organised intramolecular structures of the pearl-necklace type. In both cases, the type of the structure formed is determined by the solvent quality for the backbone and by the architectural parameters of the polymer, such as the length of the side-chains and the spacing between them. In addition to the architectural parameters the structure of the polyelectrolytes is also controlled by the degree of charging of the side-chains. The long-range nature of the electrostatic repulsion stabilises the pearl necklace structure and makes it better-defined than in the neutral combs.

Star polyelectrolytes in poor solvents

Polyelectrolyte stars are interesting systems which at a first glance might seem rather simple for theoretical description. The ease of describing the star is facilitated by its intrinsic spherical symmetry which enables to reduce the complicated three dimensional problem to quasi one-dimensional. This advantage has been used by many authors and PE stars in good solvents have been successfully modelled using mean-field models. Scaling approaches [46, 47] as well as numerical SCF modelling [48] and simulations [49] have been employed by several authors. They have shown that a PE star in good solvent has its arms stretched which is a consequence of the combination of the electrostatic repulsion among the arms of the star, osmotic pressure of the counterions which are being held inside the star volume and the steric repulsion of the arms. In the polyelectrolyte regime the dominant contribution comes from the electrostatic repulsion. In the so-called osmotic star the large number of counterions effectively screen the electrostatic repulsion and their osmotic becomes the dominant interaction. The steric repulsion among the arms of the star becomes dominant at very large number of arms. If a salt is present in the solution, it screens the electrostatics and the star size is smaller in comparison with the corresponding salt-free case.

Problems arise when one would seek a description of a PE star in a poor solvent. To make a successful theoretical description of such system, one has to anticipate what kind of structures will be formed. While in the good solvent case the spherical geometry served for key simplifications, in the poor solvent case it acts as an additional complication, as we will illustrate in the following paragraphs.

Theoretical predictions for PE stars in poor solvents

In the most naive approach one might anticipate that if a star PE is in poor solvent, it collapses uniformly, preserving its spherical symmetry. Clearly, it is very improbable that this hypothesis could be correct because there are several other ways to lower the free energy of the star. For example, individual arms of the star could respond similarly to the linear polyelectrolyte and form structures of the pearl-necklace type. Besides other factors known from the linear polyelectrolyte case, in the star geometry, the pearl size would also depend on the distance from the centre of the star.

However, the arms might also prefer to stick together due to the hydrophobic interaction and form bundles. The sticking is also favoured by counterions which gain some entropy in this way. Again, the degree of sticking might probably depend on the distance from the centre of the star which brings additional complications. The bundling effects arise due to correlations between the location of the counte-

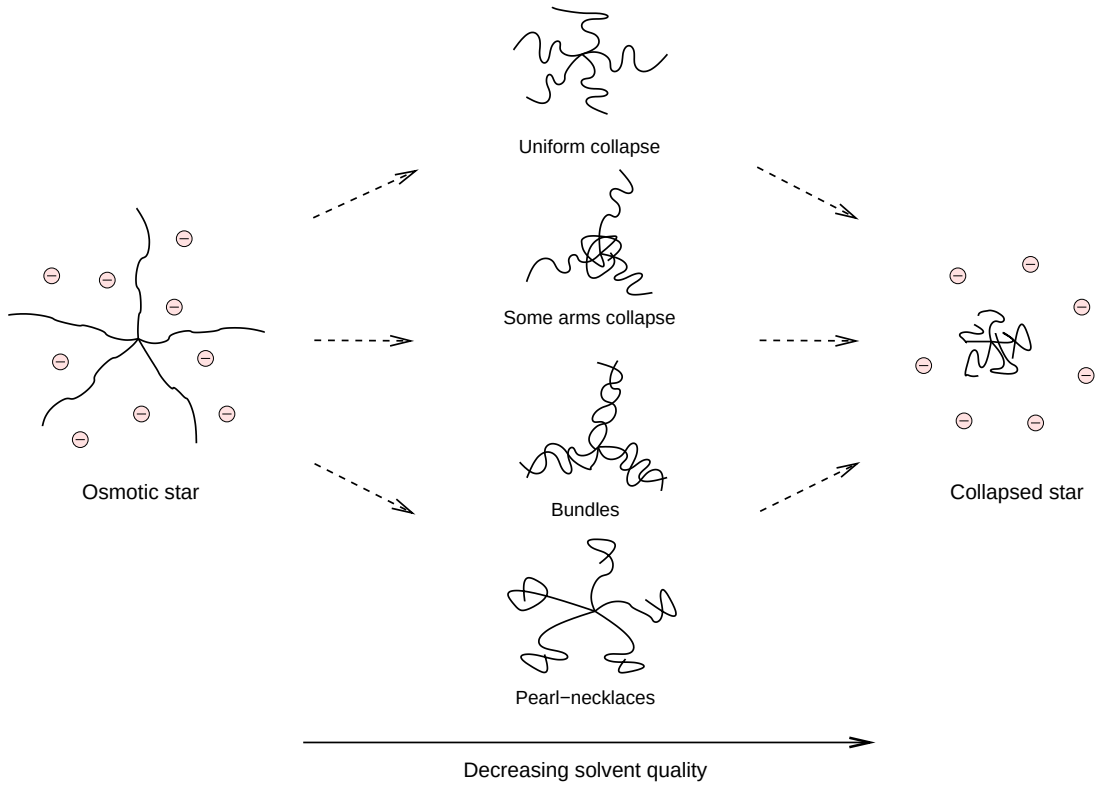

Figure 16. *Illustration of several hypothetical intermediate structures which might occur in a collapsing PE star.*

rions and the arms of the star and to make a good theoretical description of such process, one has to abandon the mean-field approximation. The arm bundling mechanism has been supported by the simulations and theoretical analysis of a similar system [8]. However, both the scaling arguments and the simulations were obtained for a model of a PE star where arms were attached to a rather large hard-sphere colloidal particle.

Another possible mechanism of the collapse of PE stars is that some arms remain stretched while others collapse close to the centre of the star. Though it might seem somewhat counter-intuitive, again this picture can be supported by scaling arguments as well as simulations made for a similar system [8]. Analogous arguments have been applied to claim that the collapse of a planar PE brush proceeds in the same way.

The different possible mechanisms of the collapse of the star upon a decrease in solvent quality are schematically illustrated in Figure 16. The two limiting regimes of the osmotic star and the collapsed star are well known and understood but the intermediate stages have not been explored yet. Though supported by physical

arguments, most anticipated structures mentioned above are a guess based on a combination of analogy and intuition. As we have demonstrated in the previous chapter, even if the guess is successful, there is always a risk that the choice of the anticipated structures is not exhaustive and there is a chance that the proper structure is not considered at all. It should be noted that there are no tools to obtain these structures from first principles, except for molecular simulations. New theoretical treatment of the collapse of a PE star in poor solvent is being developed by O. V. Borisov and collaborators. The simulation results presented here should serve as supporting information for the initial assumptions of the theory concerning the types of structures formed.

MD simulations of PE stars in poor solvents

The results described in this chapter have not been published yet. They are in the state of manuscript in preparation which we expect to submit in the fall of 2009. At the time of writing this thesis, the project has not been completely closed. Nevertheless, we find it suitable to include at least some of the results which nicely fit into the context of the rest of the thesis.

identification	number of arms	arm length	degree of charging	range of ϵ_{LJ}
5×200	5	200	0.250	0.4 – 1.4
5×400	5	400	0.250	0.4 – 1.2
10×200	10	200	0.250	0.4 – 1.4
20×100	20	100	0.250	0.4 – 1.2

Table 4. *Parameters of the simulated star polyelectrolytes.*

In Table 4 we show the different types of PE stars which we have simulated. Each of them we simulated in a range of solvent qualities starting close to θ solvent and going up to a very poor solvent. The most important structural parameters are the number of arms in the star, their length and the degree of charging. In combination with the solvent quality, ϵ_{LJ}, they determine the conformation of the star. We have chosen the parameter values so that we can observe trends induced by changes in some of them while others remain fixed. At the time of writing we have been still running simulations of some systems which are not included in this text. Similarly to the comb PE case we will refer to different stars by *(number of arms* $\times$ *arm length)* as indicated in the first column of Table 4.

Before discussing the results we would like to comment on the major technical limitation of the simulations of PE stars in poor solvents. Because the simulated polymers are rather large (thousand or more monomer units) we found it difficult to equilibrate them when they were close to the collapsed state. Specifically the equilibration was not successful when one or more arms collapsed to the centre of the polymer. In such cases the obtained conformation was largely dependent on the initial one which means that we hit a metastable state and the system was unable to find the global free energy minimum within the time of the simulation. A similar situation occurred when thick bundles were formed. For selected systems we performed a consistency check by starting the simulation with several significantly different initial conformations. We discarded those systems in which the resultant equilibrated conformation depended on the initial one. In such case it was clear that we were sampling a metastable state rather than the global free energy minimum. For each of the simulated polymers we were able to obtain reliable results up to a certain maximum value of ϵ_{LJ}. Simulation results for values of ϵ_{LJ} higher than this maximum were discarded as dubious even though they sometimes followed the expected trends.

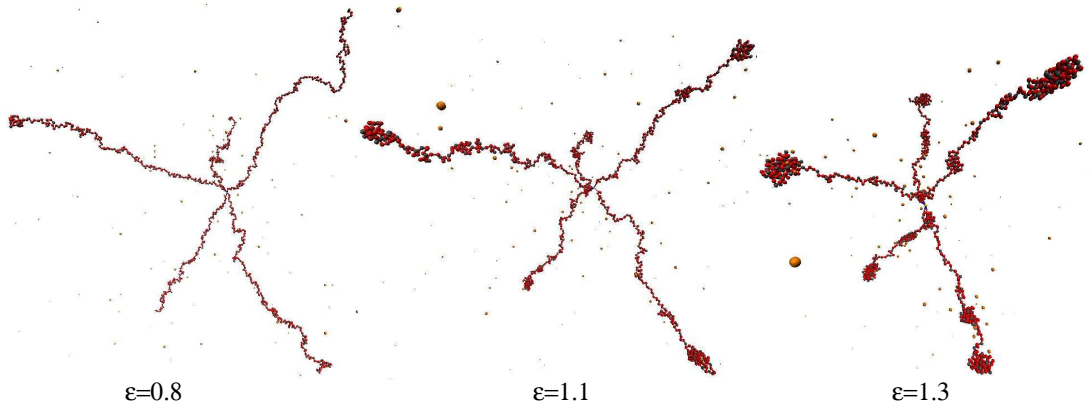

Figure 17. *Simulation snapshots of stars with 5 arms, each 200 segments long* (5×200) *for selected values of* ϵ_{LJ}*. Formation of pearl-necklace structures on individual arms with increasing* ϵ_{LJ} *can be observed. For better visibility, magnification slightly increases from left to right.*

In Figure 17 we show simulation snapshots of the (5×200) stars. They confirm one of our hypotheses, namely that pearl-necklace structures can be formed on individual arms of the PE star. In analogy with the linear PEs, the pearl size grows with decreasing solvent quality (increasing ϵ_{LJ}). However, in addition to that, it also depends on the distance from the centre of the star. For $\epsilon_{\mathrm{LJ}} = 1.1$ pearls are only formed at arm ends while for $\epsilon_{\mathrm{LJ}} = 1.3$ additional pearls are

formed on the intermediate segments of the arms, closer to the centre. The pearls closer to the centre are much smaller than the terminal ones. Deeper in the poor solvent regime we observed one or more arms collapsing to the centre of the star while others still remained stretched. Even though this seems to confirm another anticipated type of the structure and an interesting crossover from one regime to another, the results for higher ϵ_{LJ} already belong to the dubious range.

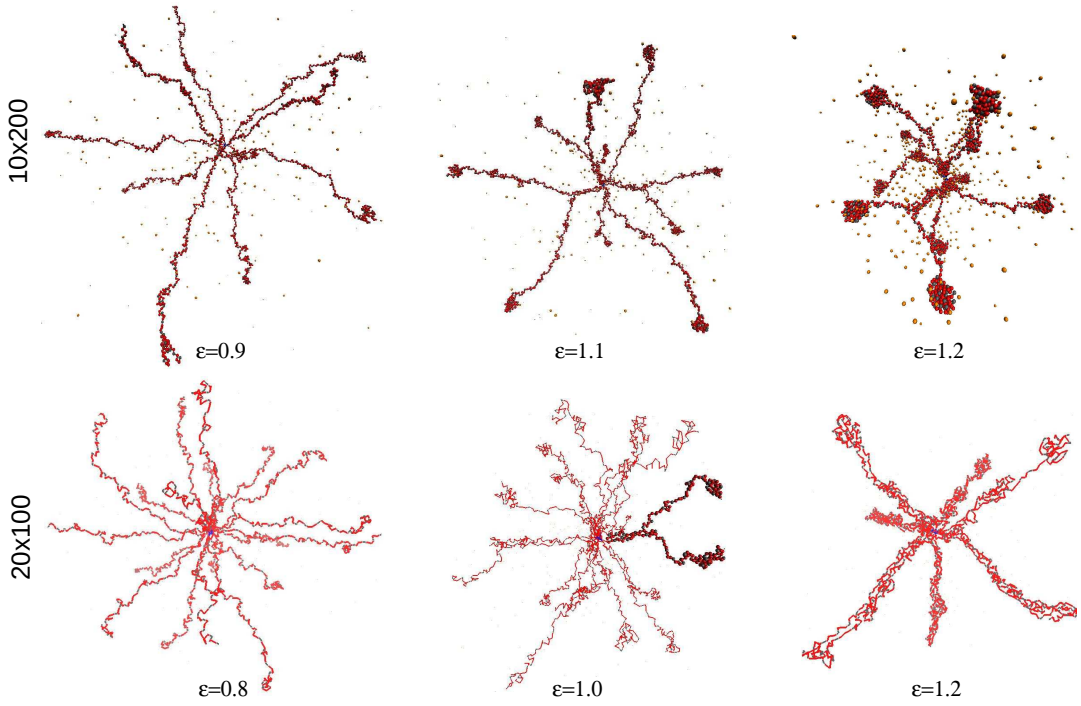

Figure 18. *Simulation snapshots of stars with 10 arms, each 200 segments long* (10×200) *and with 20 arms, each 100 segments long* (20×100) *for selected values of* ϵ_{LJ}*. Formation of bundles of arms with increasing* ϵ_{LJ} *can be observed as well as splitting of the bundles at a certain distance from the centre. For better visibility, magnification slightly increases from left to right.*

In Figure 18 we show simulation snapshots of the (10×200) and (20×100) stars. The (20×100) stars are only rendered using simple lines because they are so dense that a quasi-3D rendering makes the images messy. In all images we can observe the formation of pearls at arm ends. We can also observe bundling of arms. For smaller values of ϵ_{LJ} the bundling is only realised close to the centre and at a certain distance the bundles split, forming Y-shaped structures. It can be well seen in the (10×200) star at $\epsilon_{\mathrm{LJ}} = 1.1$. The same structural motif appears in the (20×100) star where one such structure is highlighted at $\epsilon_{\mathrm{LJ}} = 1.0$. With increasing value of ϵ_{LJ} the typical distance at which the bundles split moves

towards the outside of the star until the whole length of the arms is consumed by the bundles as shown for the (20×100) star at $\epsilon_{\mathrm{LJ}} = 1.2$. Similarly to other types of the stars, at higher values of ϵ_{LJ} we observed collapse of some arms to the centre of the star while others remained stretched and we also observed formation of thicker bundles. However, the similarity was retained also in the fact that these results again had to be discarded as dubious.

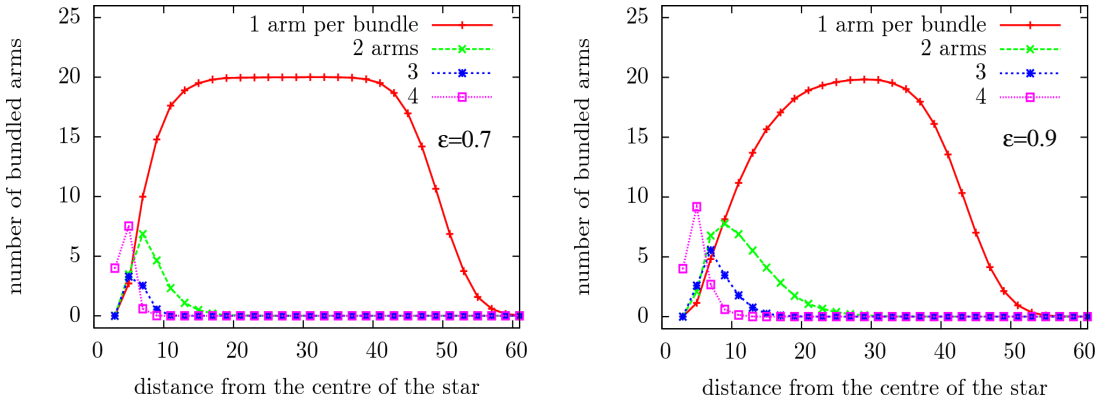

Figure 19. *Average number of arms in bundles of a given thickness as a function of the distance from the centre of the star. Data are shown fro the* (20×100) *star for* $\epsilon_{\mathrm{LJ}} = 0.7$ *and* $\epsilon_{\mathrm{LJ}} = 0.9$.

To analyse the bundling quantitatively, we have calculated average number of arms in bundles of particular thickness. By thickness of the bundle we mean the number of arms it contains. The star was divided into shells of a given width. Within each shell arms were considered as being in the same bundle if they were closer than a certain distance. This distance was arbitrarily chosen as $2.5\,\sigma_{\mathrm{LJ}}$ which was the cutoff distance of the LJ interaction. The results were found to be only weakly dependent on the width of the shells and on the distance criterion, as long as they were chosen within a reasonable range. In Figure 19 we show the plots of the average number of arms in bundles of a given thickness as a function of the distance from the centre of the star for the (20×100) star for two selected values of $\epsilon_{\mathrm{LJ}} = 0.7$ and $\epsilon_{\mathrm{LJ}} = 0.9$. In the plot on the left ($\epsilon_{\mathrm{LJ}} = 0.7$) the peak for the two-arm bundles is located much closer to the origin than the same peak in the plot on the right ($\epsilon_{\mathrm{LJ}} = 0.9$). The same holds for the other peaks which correspond to thicker bundles. Unfortunately we could not have gone too far in the poor solvent regime because when thicker bundles were formed further away from the centre, the stars had a tendency to be entrapped in metastable states.

Even though it was not possible to perform reliable simulations in which thicker bundles would be observed, we can extrapolate our observations to say that in a

sufficiently large PE star, the typical thickness of a bundle decreases as a function of the distance. An idealised picture of a conformation of a PE star might thus be some kind of dendritic structure. Starting with thick bundles close to the centre, they gradually split and get thinner with increasing distance from the central segment, eventually ending up with pearls at the very ends of individual arms, provided the arms are long enough so that the branching goes up to the last generation.

Another structure we observed in some of the simulations which were discarded as dubious are pearls on bundles. Indeed, there is no reason why there should be no pearls formed on bundles. Since it is known to have lower free energy in comparison with uniform shapes, pearls on bundles are certainly one of the structures which should be considered. Unfortunately, exploring the regime of pearls on bundles is beyond current capabilities of our simulations.

To conclude our excursion into the realm of polyelectrolyte stars we may say that there is no single regime which would properly describe the behaviour of the whole star, except for the case of low number of arms with pearl-necklaces on individual arms. For higher number of arms, based on current simulation data we propose the formation of bundles, thickness of which decreases with increasing distance from the centre, forming a dendritic structure with pearls at arm ends. Moreover, the appearance of other types of structures in the simulations which we eventually discarded suggests the possibility of crossover to other regimes which we are currently unable to explore. Obviously in PE stars in poor solvents there is a competition of several conformational regimes which should be investigated in more detail in future.

Weak polyelectrolytes in poor solvents

In the last chapter of this text we return to linear polyelectrolytes. In our very first simulation paper [31], we have simulated strong polyelectrolytes which we then compared to experimental data obtained for weak polyelectrolytes. By then it showed up that it is desirable to develop a model which would enable simulations of weak polyelectrolytes using the Molecular Dynamics (MD) simulation method. In the following years we devoted much of our effort to the development of such a model. The results contained in this chapter were published in Collection of Czechoslovak Chemical Communications in 2008 [50]. Afterwards thaw work has been continued and by now we are close to publishing another study. The new results are not included here because they are not related to intramolecular self-organised structures.

Specific features of weak polyelectrolytes

The terms *weak polyelectrolyte* and *strong polyelectrolyte* are often confused with the similar-sounding terms *weakly charged* and *strongly charged polyelectrolytes* which are commonly used by physicists. While the latter refer to the linear charge density of the polyelectrolytes, the former refer to the presence of weak or strong acid or base groups in the polymer chain. In chemical literature the term weak and strong base describes how readily the substance dissociates upon dissolution in water. While the strong acids and bases dissociate completely, the weak ones dissociate only to a certain extent. The extent to which the weak acids and bases dissociate is determined by the equilibrium dissociation constants, K_A or K_B, and by the external conditions, in particular pH and ionic strength of the solution. In the following text we will speak about acids only, bearing in mind that the behaviour of weak bases is analogous.

The dissociation and association of a weak acid is a dynamic process which takes place on time scales ranging from nanoseconds to microseconds, depending on the K_A of the acid and external conditions [51]. The event of dissociation can only be properly described on a quantum mechanical level. On the coarse-grained level it can be viewed so that the dissociation produces a charged group and a counterion out of a group which was previously uncharged. Association is the reverse process of dissociation.

The equilibrium dissociation constant, K_A, can be measured with high accuracy for a weak acid which contains one or several dissociable groups. The value of K_A

depends on the change in the Gibbs free energy upon dissociation,

$$K_{\mathrm{A}} = \exp\left(-\frac{\Delta G_{\mathrm{diss}}}{k_{\mathrm{B}}T}\right) . \tag{18}$$

The value of ΔG_{diss} of the dissociation is influenced by the presence of other charged groups in the vicinity. For example, in the case of oxalic acid, which contains two equivalent COOH groups, the equilibrium constant of dissociation of the first group is three orders of magnitude higher than that of the second group. In other words, the dissociation of the second group is strongly influenced by the presence of the other dissociated COOH group [52]. The same holds for a polymer containing weak acid groups but here the situation is more complicated. Again, the dissociation of each of the groups on the polymer chain depends on the dissociation of other groups in its vicinity. Therefore the local degree of dissociation of the polymer can be expected to be correlated with its local conformation. In particular this effect may be important in weak polyelectrolytes in poor solvents where upon a decrease in solvent quality the charged groups are brought close to each other. Experimental evidence of this effect can be found in titration experiments on poly(methacrylic acid) where changes in the effective acidity constant, K_{A}, have been observed as a function of pH [37].

Recently, simulations of weak polyelectrolytes have been performed using the Monte Carlo (MC) technique in a grand canonical ensemble [39, 40]. The results of these works have confirmed the existence of the pearl-necklace conformations also in the case of weak polyelectrolytes in poor solvents, at least in a certain range of solvent quality conditions. One might wonder why it is desirable to develop an MD simulation approach for weak PEs if they can be simulated using MC. The reason is that the two methods are complementary to a certain extent. It may be difficult to simulate locally collapsed structures such as pearl-necklaces using the MC method because different types of moves would be effective for the collapsed and for the expanded parts of the system. On the other hand, the MD method always simulates collective motions and its efficiency depends on the characteristics of the system in a different way. Last but not least, MD also provides information on time-dependent quantities which cannot be obtained from MC.

Simulations of weak polyelectrolytes using a combination of MC and MD

Because the mechanism of the dissociation/association of a weak acidic or basic group can only be properly described using quantum mechanics, to account for it on a coarse-grained level, we have to develop a suitable generic model which possesses the essential features of the underlying physical process. Our first attempt to

develop such a model was a combination MD and MC simulation methods. In this approach we had a pre-defined degree of dissociation of the polyelectrolyte which was simulated using MD. At regular intervals, the simulation run was stopped and a displacement of charge along the polymer was attempted in an MC fashion. In this move the charge from a randomly chosen charged monomer unit of the polymer was moved (if accepted) to a randomly chosen uncharged monomer unit. The technical details of the procedure are described in the original article [50]. This approach accounted for the effective mobility of the charges along the weak polyelectrolyte chain. On the other hand, the degree of charging of the polymer had a pre-defined value and therefore we could not study how it depends on external conditions such as pH. Nevertheless, this first attempt revealed important correlations between the local degree of charging of the polymer and its local conformation.

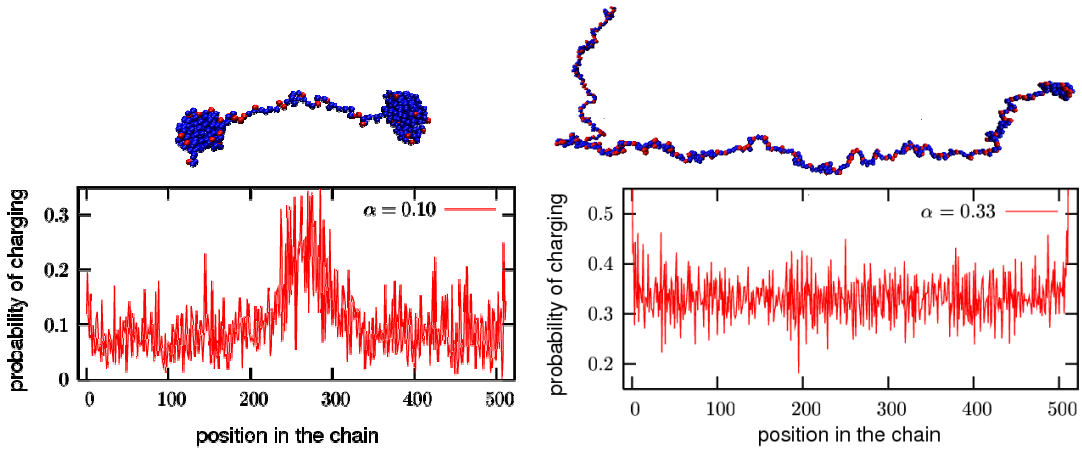

Figure 20. *Dependence of the average degree of charging on the position in the chain. Data for two different degrees of charging of a polymer with* $\epsilon_{\mathrm{LJ}} = 1.3$ *are shown. Simulation snapshots illustrate typical conformations of such polymers.*

In Figure 20 we show the plots of the average degree of charging of individual monomer units as a function of their position in the backbone. On the right, the overall pre-defined degree of charging of the polymer, $\alpha = 0.33$, is relatively high so that it adopts stretched conformation as illustrated by the simulation snapshot above the graph. In such a case the backbone is charged uniformly (apart from some noise). The only deviation is observed at the very ends where the degree of charging sharply increases. A completely different situation is observed in the case of lower degree of charging, $\alpha = 0.10$, which is shown in the left part of the figure. At this value of α the conformation is pearl-necklace, as illustrated

by the simulation snapshot, and the average local degree of charging is strongly inhomogeneous. The charges are removed from the pearls and accumulate in the strings which helps to reduce the high charge density inside the pearls. As a consequence, the local degree of charging of the pearls is lower than the average while that of the strings is significantly higher. Since the pearl-necklaces are formed even if charges are not mobile, we may conclude that the mobility of charges serves as an additional mechanism which may stabilise the pearl-necklace conformation. Moreover, the obvious correlation between the local conformation of the polymer and its local degree of charging can be extrapolated to the realm of proteins. In analogy to our system, in proteins one should expect that the effective dissociation constants of particular groups are not equal to their values for the corresponding monomers but that they depend on the local conformation of their neighbourhood.

Even though our treatment of weak polyelectrolytes in MD has provided some important results, still quite a number of unresolved methodological problems remain. For example, our simple model does not allow for transfer of charges from one polymer chain to another and therefore cannot account for the possibility of phase separation where some polymers would have a high degree of charging and remain in solution while others would have a low degree of charging and precipitate. Next, it is not clear to what extent the rate at which we apply the MC steps has an influence on the simulation. In the simulations we have performed a change in the rate by an order of magnitude in either direction. It did not significantly influence the obtained static quantities, but it influenced all time-dependent quantities.

To avoid the problems mentioned in the previous paragraph, we devoted further effort to developing a generic model of a weak PE in which dissociation is treated explicitly. In this model the weak acid and its counterion interact via a non-bonding interaction of the Lennard-Jones type. The acidity constant is controlled by the depth of the LJ interaction potential. When the potential is not too deep, the monomer-counterion pairs are only loosely kept together and dissociate readily, resulting in a high degree of dissociation. On the other hand, if the depth of the potential is higher, the weak bond is much stronger and the probability of dissociation is lower. In this model we set the dissociation constant and let the system choose its degree of charging according to the external conditions. Also, pH can be set independently and hence the dependence of various properties on pH can be studied which is much closer to experiment. The results from the explicit model of dissociation have not been published yet but we expect to publish them by the end of 2009. We do not include them in the thesis because they do not deal with the formation of intramolecular structures.

Concluding remarks

In this thesis we have shown that amphiphilic polymers can form a whole ZOO of conformational structures. We have studied the formation of such structures in several types of polymers which include neutral polymers and polyelectrolytes and several topologies, in particular linear, comb-like and star. The behaviour of all the studied systems is controlled by the balance of two counteracting forces. One of them is repulsive and brings about the expansion while the other one is attractive and brings about the collapse. As a consequence the conformation of such a polymer may contain collapsed as well as loose (expanded) domains. The size of the two types of domains is determined by the relative strength of the two counteracting forces. In our simulations we have obtained deeper insight into the features of the conformational behaviour.

In our first publication we have compared [31] our simulations of linear polyelectrolytes in poor solvents with the experimental measurements of fluorescence anisotropy decays performed about twenty years before our study [36]. The simulations have confirmed the intuitive interpretation of the experiments concerning the relation between the fluorescence anisotropy decay times and conformational changes in the polymer.

Our studies of comb-like polymers in selective solvents have been motivated by the earlier theoretical paper by Borisov and Zhulina [11]. Our simulations have qualitatively confirmed the predictions of the theory for both the neutral [12] and polyelectrolyte [13] side-chains. Moreover, especially the simulations of the neutral polymers revealed some non-trivial features of the behaviour which have not been considered by the original theory. In particular we were able to observe and explain certain effects which arise due to the finite size of the real polymers. This resulted in a joint theoretical and simulation paper and an augmented version of the theory [12]. Recently, comb-like polymers with poly(methylstyrene) backbone and poly(methacrylic acid) side-chains have been synthesised by our collaborators from the Institute of Macromolecular Chemistry of the Czech Academy of Sciences. Their conformational behaviour has been studied in our group using scattering methods and it shows up that on a qualitative level they agree with the theoretical predictions. At the time of writing this thesis we have been working on detailed interpretation of the experimental results and comparison with the simulations.

The cooperation with the theoreticians has been continued in the analysis of star polyelectrolytes in poor solvents, behaviour of which is even more complex. Our current simulation results have disclosed certain characteristics which were not anticipated before. These include the formation of bundles of chains and the fact that the thickness of the bundles depends on the distance from the centre of

the star resulting in a dendritic type of structure. We have also shown that there is a crossover from pearl-necklace behaviour in stars with low number of arms to bundling at higher number of arms. At the time of writing this thesis the project has not been completely closed.

Our simulations of the fluorescence anisotropy decays have uncovered that it would be desirable to develop a model which would enable simulations of weak polyelectrolytes using molecular dynamics (MD) [50]. We have dealt with this problem using a combination of MD and Monte Carlo (MC) method. The results have shown that the local degree of charging of a weak polyelectrolyte is correlated with its local conformation. The charge is redistributed along the polymer chain so as to oppose the increase in charge density caused by the formation of collapsed domains. The project on the weak polyelectrolytes has been continued by the development of a more sophisticated model of dissociation.

The polymers we have investigated in our simulation studies differ in many aspects. All of them, however, contain some hydrophobic parts which collapse upon a decrease in solvent quality. In all cases we have observed a transition from an expanded conformation close to theta solvent conditions through the pearl-necklace structures at poorer solvent. In the case of linear polymers the final state was found to be a single globule. In the case of comb copolymers it has been either a pearl necklace or cylinder, depending on the structural parameters of the polymer. The combs also may end up in a single spherical globule but only if the backbone is not long enough. In the case of stars we may anticipate that in the very poor solvent limit they end up in a single globule but due to technical limitations we were not able to simulate this situation.

In certain systems we could analyse in more detail some specific features of the pearl-necklace structures. One such feature are the finite-size effects which were thoroughly investigated in the case of the neutral combs. Another one is the internal organisation of the pearls which was uncovered in the comb-like polyelectrolytes. In all cases we have observed that as the solvent quality is decreased, the beginning of the pearl formation is accompanied by large fluctuations. In the region of fluctuations it is possible to observe pearls in individual conformations but their number fluctuates in time and the conformation of the polymer cannot by represented by any typical structure. This was explained by the existence of several comparably deep local minima on the free energy landscape which are separated by low barriers. Upon further decrease in solvent quality the pearls become stable and well-defined. Although all these specific features have been discussed in detail only in one or two special cases, they seem to be universal for any system which forms pearl-necklace structures.

Last but not least, there is one more property of the self-organising behaviour

analysed in our simulations which is not typical for many other self-organising systems. Normally when speaking about self-assembly, one refers to assembling molecules into supramolecular aggregates. The intermolecular self-assembly occurs only above a certain threshold concentration, the so-called critical micellar concentration (cmc). The studies presented in this thesis all deal with intramolecular self-organising behaviour which is supposed to occur within one macromolecule in the dilute solution limit. The morphology of the intramolecular aggregates is controlled by the structure of the polymer and by the external conditions such as the solvent quality, ionic strength or pH. In this respect it is very similar to the self-organising behaviour of proteins. Although they are much more complex than our simple polymers, we may claim that the behaviour of proteins is governed by the same physical principles and hence from our simulation results we can also try to understand the behaviour of the complex biomacromolecules.

Summary

In this thesis we have presented results of our simulation studies concerning the intramolecular morphology of amphiphilic polymers. Amphiphilic polymers are those which contain two or more types of monomer units with different affinity for the solvent. Using the common terminology of polymer physics, we say that such polymers are in the selective solvent, i. e. such that it is poor for one type of units and good for the other type. In our definition of amphiphilic polymers we also include polyelectrolytes in which the good solvent conditions can be induced by the electrostatic repulsion among the charged monomer units. In our studies we have investigated both polyelectrolytes and neutral polymers of linear as well as branched topologies.

While the poorly soluble monomer units have the tendency to collapse into compact globular structures, this tendency is counteracted by the excluded volume repulsion among the well-soluble units. Equilibrium is attained when the two tendencies are balanced which often results in the so-called pearl-necklace conformation consisting of both collapsed domains (pearls) and stretched ones (strings). This behaviour has been first predicted for linear polyelectrolytes in poor solvents by Dobrynin and coworkers [8]. Later on similar structures have been predicted by various authors including ourselves for a whole variety of different amphiphilic polymers. Besides pearl-necklaces, for the branched macromolecules also other types of structures have been predicted, as we will discuss further.

In all our studies we have used Molecular Dynamics in implicit solvent as our simulation method. Besides structural parameters of the polymers one of the key parameters has been the solvent quality. It was controlled via the depth of the Lennard-Jones interaction among the monomer units, ϵ_{LJ}, which was usually varied in the range from close-to-theta conditions down to very poor solvent $0.3 \leq \epsilon_{\mathrm{LJ}} \leq 2.0$.

Our very first study [31] dealt with the pearl-necklace structures in linear polyelectrolytes in poor solvents. Besides the morphological study we compared our simulation data with the experimental measurements of fluorescence anisotropy decays [36]. On the semi-quantitative level our simulation confirmed the intuitive interpretations of the relations between the changes in the fluorescence anisotropy decay times and the conformational changes in the polymer.

Our studies of comb-like copolymers in selective solvents were motivated by the publication of the scaling analysis of neutral combs in selective solvents by Borisov and Zhulina in 2005 [11]. Their treatment predicted the formation of pearl-necklace structures, cylindrical and spherical intramolecular micelles and lamellar structures. We anticipated that similar behaviour should be observed

if the side-chains are polyelectrolytes which was confirmed by simulations [13]. Afterwards we started an intensive cooperation with the theoreticians. It resulted in a joint publication which contained both the simulations and an augmented version of the scaling theory [12]. The results confirmed the main qualitative trends of the original theoretical treatment but they also showed that it did not describe properly the region where the pearl-necklace structures start to be formed and the limit of very poor solvent.

The fruitful cooperation has been continued in the study of star polyelectrolytes in poor solvents. In this case the simulations revealed a very complex behaviour. At low number of arms pearl-necklace structures are formed on individual arms of the star. When the number of arms is increased, they form bundles. The number of arms in the bundle is highest close to the centre of the star and decreases with increasing distance from the centre forming a dendritic structure with pearls at the ends of individual arms.

In our fisrt study we were comparing our simulation results obtained for a polyelectrolyte with fixed and uniform degreee of charging with experiments performed on a weak polyelectrolyte. In a weak polyelectrolyte the degree of charging is variable and is determined by the pH of the solution. We anticipated that if a weak polyelectrolyte is found under poor solvent conditions where the pearl-necklace structures are formed, its degree of charging need not be uniform along the whole chain. We used a combination of molecular dynamics and Monte Carlo simulation methods to simulate a polymer in which the degree of charging of individual monomer units was allowed to vary so that the overall degree of charging of the polymer remained constant. It showed up that if such polymer is found in the stretched conformation, its degree of charging is almost uniform. On the other hand, if it is found in the pearl-necklace conformation, the stretched parts of the chain (strings) have a much higher degree of charging than the collapsed parts (pearls). We have concluded that the mobility of charges serves as an additional mechanism of stabilising the pearl-necklace structure.

In conclusion we may say that from our simulations we have seen that the self-organising behaviour at the single molecule level is not only the domain of biomacromolecules but it can also be observed in much simpler synthetic systems. We have also shown that certain physical principles which govern the self-organising behaviour are universal. Their detailed understanding in the simple systems can besides other things help to understand the behaviour of the more complex biological molecules such as proteins.

Shrnutí

Tato práce obsahuje výsledky simulačních sutdií, které se zabývají intramolekulární morfologií amfifilních polymerů. Pod pojmem amfifilní se rozumí takový polymer, který obsahuje dva nebo více typů monomerních jednotek s různou afinitou vůči rozpouštědlu. V rámci polymerní fyziky pak mluvíme o tzv. selektivním rozpuštědle, t.j. takovém, které je dobré pro jeden druh monomerních jednotek a špatné pro druhý. V tomto textu budeme mezi amfifilní polymery zahrnovat i polyelektrolyty, u kterých jsou podmínky dobrého rozpouštědla dosaženy nepřímo skrze repulzi nabitých monomerních jendotek. V našich studiích jsme se zabývali jak polyelektrolyty, tak neutrálními polymery, které měly lineární nebo větvenou strukturu.

Špatně rozpustné monomerní jednotky mají tendenci kolabovat a tvořit kompaktní globulární struktury. Proti této tendenci působí repulze pocházející od vyloučeného objemu dobře rozpustných monomerních jednotek. V rovnováze jsou tyto dvě tendence navzájem vykompenzovány, přičemž často vznikají tzv. struktury perlového náhrdelníku (anglicky pearl-necklace structures). Tyto struktury obsahují jak kolabované domény (perličky) tak i natažené (řetízky). Tento typ chování poprvé popsali Dobrynin a kol. [8]. Později byl vznik podobných struktur předpovězen různými autory pro celou škálu rozmanitých amfifilních polymerů. Pro větvené makromolekuly byly kromě perlového náhrdelníku předpovězeny ještě jiné struktury, které budou zmíněny dále.

Ve všech našich simulačních studiích jsme používali simulační metodu molekulové dynamiky v implicitním rozpouštědle. Kromě strukturních parametrů polymerů hrála ve všech simulacích klíčovou roli také kvalita rozpouštědla. Tu jsme v simulacích nastavovali pomocí hloubky Lennardova-Jonesova potenciálu, ϵ_{LJ}, kterým byla popsána interakce mezi monomerními jednotkami. Hodnotu ϵ_{LJ} jsme měnili v rozsahu od hodnot, které téměř odpovídají θ rozpouštědlu, až po velmi špatné rozpouštědlo, $0.3 \leq \epsilon_{\mathrm{LJ}} \leq 2.0$.

V naší první publikaci [31] jsme studovali vznik perličkových struktur u lineárních polyelektrolytů ve špatných rozpoštědlech. Kromě morfologické studie jsme srovnávali naše data ze simulací s experimenty, které byly provedeny v naší laboratoři před cca dvaceti lety [36]. Na semikvantitativní úrovni naše simulace potvrdily intuitivní interpretaci vztahu mezi vyhasínáním anizotropie fluorescence a konformačními změnami polymeru.

Naše studie hřebenových polymerů v selektivních rozpouštědlech byly inspirovány teoretickou analýzou neutrálních hřebenových kopolymerů, kterou publikovali Borisov a Zhulina v roce 2005 [11]. V této práci předpověděli vznik perličkových struktur, cylindrických i sférických intramolekulárních micel a lamelár-

ních struktur. Předpokládali jsme, že podobné chování by mohlo být pozorováno v případě, že postranní řetězce budou tvořeny polyelektrolyty, což jsme také potvrdili pomocí simulací [13]. V pozdější době jsme s výše zmíněnými teoretiky začali úzce spolupracovat. Výsledkem této spolupráce je společná publikace, ve které jsou obsaženy výsledky simulací i rozšířená verze původní teorie pro neutrální hřebeny [12].

Úspěšná spolupráce dále pokračovala studiem hvězdicových polyelektrolytů ve špatných rozpouštědlech. V tomto případě simulace ukázaly velmi komplexní chování. Při nízkém počtu ramen vznikají perličkové struktury na jednotlivých ramenech. Když je počet ramen vyšší, tvoří se svazky. Počet ramen ve svazku je nejvyšší v blízkosti středu hvězdice a s rostoucí vzdáleností od středu klesá, čímž vzniká dendritická struktura s perličkami na koncích jednotlivých ramen.

V naší první práci jsme srovnávali simulační data pro polyelektrolyt s předem daným stupněm disociace s experimenty provedenými na slabých polyelektrolytech. V případě slabého polyelektrolytu je ale stupeň disociace variabilní a závisí na pH roztoku. Předpokládali jsme, že když se slabý polyelektrolyt nachází ve špatném rozpouštědle za podmínek, kdy vznikají perličkové struktury, jeho stupeň disociace nemusí být stejný po celé délce řetězce. S použitím kombinace metod molekulové dynamiky a Monte Carlo jsme simulovali polymer, u kterého bylo možno lokálně měnit stupeň disociace tak, že celkový stupeň disociace zůstal konstantní. Ukázalo se, že pokud takový polymer zaujme nataženou konformaci, stupeň disociace je téměř rovnoměrně rozložen podél řetězce. Na druhé straně, pokud se polymer nachází v perličkové konformaci, natažené části řetězce (řetízky) mají výrazně vyšší stupeň disociace než kolabované perličky. Z toho jsme usuzovali, že pokud se náboj může pohybovat po řetězci, je to další možný způsob, jak stabilizovat perličkovou strukturu.

Závěrem můžeme říci, ze z různých našich simulací se ukazuje, že samoorganizující chování na intramolekulární úrovni není pouze doménou biomakromolekul, ale lze jej pozorovat i u mnohem jednodušších syntetických polymerů. Ukázali jsme také, že některé fyzikální principy, které podmiňují samoorganizující chování, jsou univerzální. Jejich důkladné pochopení u jednoduchých systémů může kromě jiného pomoci také k lepšímu chápání chování složitých biomakromolekul.

Acknowledgement

In the first place, I would like to thank my supervisors prof. Karel Procházka and doc. Zuzana Limpouchová for working with me since I started to work in the lab as a diploma student. My thanks also belong to my colleagues from the lab with who I have been working on everyday problems in simulations, namely Filip Uhlík, Jitka Kuldová and Karel Jelínek. I also have to express my thanks to our foreign collaborators who have provided different points of view of the subjects we have been studying together. In particular, these are Oleg V. Borisov, Frans Leermarkers and Marat Charlaganov. Last but not least, I would like to thank my wife for support, especially in the last few days of writing the thesis.

The funding for the work included in the thesis came from a number of resources. In the first place it was the POLYAMPHI project of the Marie Curie Research and Training network, thanks to which I could spend a couple of months in the labs in Wageningen and Pau and started a cooperation which has been continued until now. Another general-purpose funding came from the Ministry of Education, Youth and Sports of the Czech republic, project MSM0021620857 and the Grant Agency of the Czech Republic, project GD203/05/H001. Funding for specific research was provided by the Grant Agency of the Czech Academy of Sciences, projects KJB40111701 (Weak polyelectrolytes), IAA400500703 (Neutral branched polymers) and IAA40110702 (Star polyelectrolytes). Another portion of the funds came from the Grant Agency of the Czech Republic, project 203/07/0659 (Branched polyelectrolytes) and the Grant Agency of the Charles University in Prague (Persistence length of polyelectrolytes). Most simulations were performed using the computational resources of METACentrum provided within the framework of the long-term research plan MSM6383917201.

References

1 P. J. Flory, Principles of Polymer Chemistry, Cornell University Press, New York, 1953.

2 P. Munk, T. M. Aminabhavi, Introduction to macromolecular science, 2nd edition, John Wiley & sons, New York, 2002.

3 M. Rubinstein, R. H. Colby, Polymer Physics, Oxford University Press, New York, 2003.

4 A. Yu. Grosberg, A. R. Khokhlov, Statistical Physics of Macromolecules, AIP Press, London, 1994.

5 P. G. de Gennes, Scaling concepts in Polymer Physics, Cornell University Press, Ithaca, 1979.

6 M. Charlaganov, P. Košovan, F. A. M. Leermarker„ Soft Matter **5** (2009) 1448.

7 A. R. Khokhlov, Journal of Physics A – Mathematical and General **13** (1980) 979.

8 A. V. Dobrynin, M. Rubinstein, S. P. Obukhov, Macromolecules **29** (1996) 2974.

9 H. J. Limbach, C. Holm, Journal of Physical Chemistry B **107** (2003) 8041.

10 H. J. Limbach, C. Holm, Journal of Chemical Physics **114** (2001) 9674.

11 O. V. Borisov, E. B. Zhulina, Macromolecules **38** (2005) 2506.

12 P. Košovan, J. Kuldová, Z. Limpouchová, K. Procházka, E. B. Zhulina, O. V. Borisov, Macromolecules **42** (2009) 6748.

13 P. Košovan, Z. Limpouchová, K. Procházka, Journal of Physical Chemistry B **111** (2007) 8605.

14 D. J. Sandberg, J. M. Y. Carrillo, A. V. Dobrynin, Langmuir **23** (2007) 12716.

15 P. Košovan, J. Kuldová, Z. Limpouchová, K. Procházka, E. B. Zhulina, O. V. Borisov, (article in preparation).

16 V. Hugouvieux, M. A. V. Axelos, M. Kolb, Macromolecules **42** (2009) 392.

17 M. P. Allen, D. J. Tildesley, Computer simulation of liquids, Clarendon Press, Oxford, 1987.

18 D. Frenkel, B. Smit, Understanding molecular simulation, Academic Press, San Diego, 1996.

19 H. J. C. Berendsen, Simulating the Physical World: hierarchical modeling from quantum mechanics to fluid dynamics, Cambridge University Press, Cambridge,

2007.

20 D. C. Rapaport, The art of molecular dynamics simulation, Cambridge University Press, Cambridge, 1995.

21 K. Binder (ed.), Monte Carlo and Molecular Dynamics Simulations in Polymer Science, Oxford Univ. Press„ New York, 1995.

22 M. Praprotnik, L. Delle Site, K. Kremer, Annual Review of Physical Chemistry **59** (2008) 545.

23 P. Hünenberger, Advances in Polymer Science **173** (2005) 105.

24 `http://www.espresso.mpg.de/`

25 Limbach, H.-J., Arnold, A., Mann, B. A., Holm, C., Computer Physics Communications **174** (2006) 704.

26 U. Micka, C. Holm, K. Kremer, Langmuir **15** (1999) 4033.

27 T. Darden, D. York, L. Pedersen, Journal of Chemical Physics **98** (1993) 10089.

28 P. P. Ewald, Annalen der Physik **64** (1921) 253.

29 M. Deserno, C. Holm, Journal of Chemical Physics **109** (1998) 7678.

30 M. Deserno, C. Holm, Journal of Chemical Physics **109** (1998) 7694.

31 P. Košovan, Z. Limpouchová, K. Procházka, Macromolecules **39** (2006) 3458.

32 J. R. Lakowicz, Principles of fluorescence spectroscopy, 3rd ed., Springer, New York, 2006.

33 J. R. Lakowicz (ed.), Topics in fluorescence spectroscopy, Vol. 1–7, Kluwer Academic / Plenum Publishers, New York, 1991–2003.

34 P. Košovan, Molecular Dynamics Simulations of Fluorescence Anisotropy from Labeled Polyelectrolyte Chains (diploma thesis), Charles University in Prague, Prague, 2005.

35 A. Szabo, Journal of Chemical Physics **81** (1984) 150.

36 Z. Limpouchová, K. Procházka, V. Fidler, J. Dvořàk, B. Bednář, Collection of Czechoslovak Chemical Communications **58** (1983) 213.

37 C. Heitz, M. Rawiso, J. François, Polymer **40** (1999) 1637.

38 E. Raphael, J.-F. Joanny, Europhysics Letters **13** (1990) 623.

39 S. Uyaver, C. Seidel, Journal of Physical Chemistry B **108** (2004) 18804.

40 S. Uyaver, C. Seidel, Europhysics Letters **64** (2003) 536.

41 S. Ulrich, A. Laguecir, S. Stoll, Journal of Chemical Physics **122** (2005) 094911.

42 A. Laguecir, S. Ulrich, J. Labille J, N. Fatin-Rouge, S. Stoll, J. Buffle, European Polymer Journal **42** (2006) 1135.

43 T. M. Birshtein, O. V. Borisov, E. B. Zhulina, A. R. Khokhlov, T. A. Yurasova, Polym. Sci. USSR **29** (1987) 1293.

44 The simulation movie can be downloaded from the supporting information of the paper P. Košovan, J. Kuldová, Z. Limpouchová, K. Procházka, Zhulina, E. B., Borisov, O. V., Macromolecules **42** (2009) 6748 or from the web page `http://lynette.natur.cuni.cz/research`

45 O. Jagodzinski, E. Eisenrigler, K. Kremer, Journal de Physique (France) **2** (1992) 2243.

46 O. V. Borisov, Journal de Physique II **6** (1996) 1.

47 O. V. Borisov, E. B. Zhulina, European Physical Journal **4** (1998) 205.

48 J. K. Wolterink, Polyelectrolytes behaviour in solutions and at interfaces (dissertation), Wageningen University, Wageningen, 2003.

49 A. Jusufi, C. N. Likos, M. Ballauff, Colloid and Polymer Science **282** (2004) 910.

50 P. Košovan, Z. Limpouchová, K. Procházka, Collection of Czechoslovak Chemical Communications **73** (2008) 439.

51 C. H. Bamford, C. F. Tripper (eds.), Comprehensive Chemical Kinetics, Vol. 8: Proton Transfer, Elsevier, Amsterdam, 1977.

52 J. Vohlídal, A. Julák, K. Štulík, Chemické a analytické tabulky, Grada publishing, Praha, 1999.

Appendices – reprints of published articles

Copyright notice

Appendix A

Molecular Dynamics Simulations of Fluorescence Anisotropy Decays from Labeled Polyelectrolyte Chains.

Peter Košovan, Zuzana Limpouchová and Karel Procházka

Macromolecules, 39 2006 3458
DOI: 10.1021/ma052557a

Appendix B

Conformational Behavior of Comb-like Polyelectrolytes in Selective Solvent: Computer Simulation Study

Peter Košovan, Zuzana Limpouchová and Karel Procházka

Journal of Physical Chemistry B 111 2007 8605
DOI: 10.1021/jp072894g

Appendix C

Amphiphilic Graft Copolymers in Selective Solvents: Molecular Dynamics Simulations and Scaling Theory

Peter Košovan, Zuzana Limpouchová, Jitka Kuldová Karel Procházka, Oleg V. Borisov and Ekaterina B. Zhulina

Macromolecules 42 2009 6748
DOI: 10.1021/ma900768p

Appendix D

Charge Distribution and Conformations of Weak Polyelectrolyte Chains in Poor Solvents

Peter Košovan, Zuzana Limpouchová and Karel Procházka

Collection of Czechoslovak Chemical Communications 73 2008 439
DOI: 10.1135/cccc20080439